

---

This is the **published version** of the master thesis:

Korcum, M. Koray; Zamora González, Gerard , dir.; Bonache Albacete, Jordi , dir. High directive antennas based on metamaterials. 2019. 66 pag. (1170 Màster Universitari en Enginyeria de Telecomunicació / Telecommunication Engineering)

---

This version is available at <https://ddd.uab.cat/record/259424>

under the terms of the  license



Master's Thesis

**Master in Telecommunication Engineering**

---

**High Directive Antennas Based on Metamaterials**

M. Koray Korcum

---

Supervisor: Gerard Zamora González, Jordi Bonache Albacete

*Departament d'Enginyeria Electrònica*

**Escola d'Enginyeria (EE)**

**Universitat Autònoma de Barcelona (UAB)**

July 2019



El sotasignant, *Gerard Zamora González i Jordi Bonache Albacete*, Professor de l'Escola Tècnica Superior d'Enginyeria (ETSE) de la Universitat Autònoma de Barcelona (UAB),

CERTIFICA:

Que el projecte presentat en aquesta memòria de Treball Final de Master ha estat realitzat sota la seva direcció per l'alumne *M. Koray Korcum*.

I, perquè consti a tots els efectes, signa el present certificat.

Bellaterra, *Miércoles, 10 de julio de 2019*

Signatura: *Gerard Zamora González i Jordi Bonache Albacete*

**Resum:**

*En aquest estudi, ens centrem en el disseny d'una antena alta directivitat basada en tecnologia de metamaterial. Aprofitant les propietats especials dels metamaterials, vam aconseguir mitjans compostos que es comporten de manera homogènia. En utilitzar aquest mitjà, vam dissenyar estructures periòdiques que es poden modificar per aconseguir una antena que proporciona una alta directivitat. Vam decidir utilitzar l'Antena leaky-Wave (LWA), dissenyada amb base en tecnologia "microstrip" composta per CSRRs. El nostre disseny d'Antena "leaky wave" (LWA) pot aconseguir una alta directivitat i funciona en règim esquerr. El disseny LWA proposat destinat a les aplicacions pot funcionar en freqüències curtes i baixes, com les aplicacions Bluetooth que s'utilitzen comunament en entorns urbans.*

**Resumen:**

*En este estudio, nos centramos en el diseño de una antena de alta directividad basada en tecnología de metamaterial. Aprovechando las propiedades especiales de los metamateriales, logramos medios compuestos que se comportan de manera homogénea. Al utilizar este medio, diseñamos estructuras periódicas que se pueden modificar para lograr una antena que proporciona una alta directividad. Decidimos usar la Antena Leaky-Wave (LWA), diseñada con base en tecnología "microstrip" compuesta por CSRRs. Nuestro diseño de Antena de Onda "Leaky wave" (LWA) puede lograr una alta directividad y funciona en régimen zurdo. El diseño LWA propuesto destinado a las aplicaciones puede funcionar en frecuencias cortas y bajas, como las aplicaciones Bluetooth que se utilizan comúnmente en entornos urbanos.*

**Summary:**

*In this study, we focused on designing a High directive antenna based on metamaterial technology. Taking advantage of the special properties of metamaterials, we achieved composite media that behaves as a homogenous. While using this media we designed periodic structures which can be modified to achieve an antenna that provides high directivity. We decided to use Leaky-Wave Antenna (LWA), designed based on microstrip technology composed with CSRRs. Our Leaky-Wave Antenna (LWA) design can achieve high directivity and works in Left-handed regime. Proposed LWA design aimed for the applications can work in short range and low frequencies, like for Bluetooth applications that commonly used in urban environments.*

“Hayatta en hakiki mürşit ilimdir. İlim ve fenden başka yol gösterici aramak gaflettir,  
dalalettir, cehalettir...”

- **Mustafa Kemal ATATÜRK**

## Table of Contents

1. Introduction and Objectives .....	1
2. Introduction to Metamaterials .....	3
2.1 Electromagnetic Crystals (EBGs) .....	4
2.2 Effective Media .....	5
3. Effective Three-Dimensional Media .....	7
3.1 Introduction to Split Ring Resonators (SRR).....	7
3.2 Introduction to Complementary Split Ring Resonators (CSRR) .....	10
3.3 Negative Effective Permeability Media (MNG) .....	12
3.4 Negative Effective Permittivity Media (ENG).....	13
3.5 Left-Handed Media (LHM).....	15
3.5.1 Propagation of Waves in LH Media.....	16
4. Metamaterial Transmission Lines .....	19
4.1 The Dual (Backward) Transmission Line Concept .....	22
4.2 Composite Right-Left Handed Transmission Lines (CRLH).....	26
4.2.1 Transmission Lines Based on Split Ring Resonators (SRRs) .....	29
4.2.2 Transmission Lines Based on Complementary Split Ring Resonators (CSRRs) 32	
5. Metamaterial Based Leaky-Wave Planar Antenna Design for Bluetooth Applications .....	33
5.1 Leaky-Wave Antennas Based on Metamaterial Transmission Lines.....	34
5.2 The Bluetooth Technology .....	40
5.3 Proposed Structure .....	41
5.4 Simulations and Experimental Results.....	44
6. Conclusions .....	56
References .....	58

## Table of Figures

Figure 1 The negative refractive index of Metamaterial (on the right) versus Conventional Material (on the left). .....	3
Figure 2 Classification of microwave metamaterials constructions. Figure extracted from [2] ...	4
Figure 3 Classification of materials according to $\epsilon$ and $\mu$ . Figure edited from [3].....	6
Figure 4 Split Ring Resonator (SRR). Figure edited from [8] .....	8
Figure 5 Electric and Magnetic fields demonstration of Coplanar Waveguide transmission line	8
Figure 6 SRR and its Equivalent circuit Model. Figure edited from [10].....	9
Figure 7 Complementary split ring resonators (CSRR). [8] .....	10
Figure 8 Electric and Magnetic fields demonstration of microstrip transmission line.....	11
Figure 9 CSRR and its Equivalent circuit Model. Figure edited from [10] .....	11
Figure 10 Artificial MNG media corresponds with array of SRRs that constitutes an effective permeability.....	12
Figure 11 Effective permeability as a function of frequency. Figure edited from [12]. .....	13
Figure 12 Artificial wire media exhibiting negative effective permittivity. Figure edited from [5]. .....	14
Figure 13 Effective permittivity as a function of frequency. Figure edited from [12]. .....	15
Figure 14 Effective left-handed artificial media (LHM) formed by a combination of ENG and MNG medias. Figure extracted and edited from [3]. .....	16
Figure 15 The refractive index of two different medias.....	16
Figure 16 Directions of $S, E, H, \beta, Vg$ and $Vp$ Vectors for both RHM and LHM. Figure extracted from [14]......	18
Figure 17 Generation of a forward (a) and backward (b) leaky wave in a periodic structure. Figure extracted from [14] .....	20
Figure 18 (a) Unit cell of TL, (b) Lumped elements of the unit cell, (c) Periodic artificial TL composed of cascading the identical unit cells (UC). Figure extracted from [11].....	21
Figure 19 Equivalent circuit model of backward TL (a) and forward TL (b) respectively. The T-circuit models of the unit cell structures for backward TR (c) and forward TR (d). Figure extracted from [6]......	22
Figure 20 Dispersion diagram for forward (a) and backward (b) transmission line models and Bloch impedance with cut-off frequency for forward (c) and backward lines (d). Figure extracted from [6]......	24
Figure 21 A unit cell of the CRLH transmission line. Figure extracted from [6] .....	27
Figure 22 General dispersion diagram of Unbalanced CRLH TR (a) Bloch impedance change with frequency (b). Figure extracted from [5]......	28
Figure 23 General dispersion diagram of Balanced CRLH TR (a) Bloch impedance change with frequency (b). Figure extracted from [5].....	29
Figure 24 Distribution of the electric field lines (in blue) and magnetic field (in red) of a Coplanar Waveguide (CPW) line. Figure edited from [14]. .....	30
Figure 25 The layout of the CPW transmission line loaded with SRRs. Figure extracted from [13]......	30
Figure 26 Equivalent circuit model for the unit cell of CPW loaded with SRR, the structure from Figure 26 (a) and the transformed version (b). Figure extracted from [5] .....	31
Figure 27 Distribution of electric field lines (in blue) and magnetic field (in red) of microstrip line. Figure edited from [14]. .....	32

Figure 28 The layout of the microstrip transmission line loaded with CSRRs. Figure extracted from [13] .....	33
Figure 29 Equivalent circuit model for the unit cell of the microstrip line loaded with CSRR. Figure extracted from [14] .....	33
Figure 30 Dispersion Diagram of LWA with the possible directions of radiations. Figure extracted from [16].....	36
Figure 31 Typical metamaterial structure without losses shown. The signal travels inside the metamaterial has a wave number $\beta$ while the signal radiated to the air has a wave number $k_0$ . Figure extracted from [17]. .....	36
Figure 32 General dispersion diagram of a balanced CRLH transmission line and 4 main regions. Figure extracted from [5].....	37
Figure 33 Dispersion diagram of the SRR loaded CPW unit cell. Figure extracted from [19]...	39
Figure 34 A unit cell of CRLH transmission line. Figure extracted and edited from [19].....	39
Figure 35 The simulated a) and measured normalized b) radiation patterns of the designed CRLH TR in different frequencies. Figure extracted from [19]. .....	40
Figure 36 Equivalent circuit model for the unit cell of the microstrip line loaded with CSRR. Figure extracted from [14]. .....	42
Figure 37 Dispersion diagram of Unbalanced CRLH TR. Figure extracted and edited from [5]. .....	43
Figure 38 Frequency analysis of an LWA based on an unbalanced CRLH (on the top) and balanced CRLH (on the bottom) TR loaded with CSRR. Figure extracted and edited from [18]. .....	44
Figure 39 Substrate design of the microstrip transmission line loaded with CSRR.....	45
Figure 40 LH Unit cell design layout.....	45
Figure 41 S-parameters of the LH unit cell.....	47
Figure 42 Equations for to achieve the unit cell characteristic parameters .....	47
Figure 43 LH unit cell characteristic parameters .....	48
Figure 44 Dissipated Power Equation.....	49
Figure 45 LWA with 25-unit cells layout, with total length 44,25 cm. ....	49
Figure 46 LWA with 25-unit cells characteristics.....	50
Figure 47 Simulated 3D radiation diagram of the resulting 25 cells LWA, calculated at 2.448 GHz. ....	50
Figure 48 Normalized representation of the gain, directivity and radiation angle of the 25 Unit Cells LWA. ....	51
Figure 49 LWA with 40-unit cells characteristics.....	52
Figure 50 Simulated 3D radiation diagram of the resulting 40 cells LWA, calculated at 2.448 GHz. ....	52
Figure 51 Normalized representation of the gain, directivity and radiation angle of the 40 Unit Cells LWA. ....	53
Figure 52 LWA with 50-unit cells characteristics.....	53
Figure 53 Simulated 3D radiation diagram of the resulting 50 cells LWA, calculated at 2.448 GHz. ....	54
Figure 54 Normalized representation of the gain, directivity and radiation angle of the 50 Unit Cells LWA. ....	54



## 1. Introduction and Objectives

In this study we aimed to design a High directive antenna based on metamaterial technology. In last two decades metamaterial technology had become popular in investigations and applications in electromagnetic engineering field. In this study, we will take an advantage of this technology to design a high directive antenna.

Metamaterials are such an artificial structure that commonly used in electromagnetic field. The reason why will use the metamaterials in this project is that metamaterials are capable to provide negative values of some electromagnetic properties like permeability and permittivity. Metamaterials are considered as effective media since the length of their elementary unit cells is much smaller than the wavelength., so that the variation of the wave that a unit cell perceives is insignificant. Some of those media can be implemented by means of resonant structures that have a quasi-static resonance, if the unit cells length of the media has very small dimensions in terms of  $\lambda$ . The first developed effective media presented as a three-dimensional structure which complicated its integration to other technologies and greatly limited the applications where they could be used. However, development of the planar technology, effective media allowed to give a more attractive approach for the microwave engineering sector, in terms of integration and compatibility of effective media with planar technologies.

Many antennas are designed to radiate electromagnetic waves in a single direction or over a narrow-angle. The power density of the antenna radiates in the direction of its strongest emission and the degree to which the radiation emitted is concentrated in a single direction. The directivity of an antenna measured from the direction of its strongest emission in radiation. To achieve high directivity, we need to design an antenna which should be long enough to have a high directivity. Based on this we want to design an antenna which can detect a certain area defined.

There are different types of antennas we can use to achieve high directivity. An array antenna can achieve higher directivity, that is a narrower beam of radio waves. But, Array antennas use large number of individual antenna elements to make the gain higher and the beam narrower, this reason makes the array antennas more complexity to implement, design and feed. However, Leaky-Wave Antenna (LWA), are much easier in

terms of complexity to implement, design and feed. Leaky-Wave Antennas (LWA) use a traveling wave on a guiding structure as the main radiating mechanism. Leaky-Wave Antenna has a phase velocity greater than the speed of light. This type of wave radiates continuously along the whole length of structure. With this type of antenna highly directive beams can be achieved at an arbitrary specified angle. The phase constant  $\beta$  of the wave controls the beam angle while the attenuation constant  $\alpha$  controls the beamwidth and those values can be varied with changing the frequency.

The project presents the design and implementation of a Leaky-Wave Antenna (LWA), which operates at 2.4 GHz, taking advantage of effective planar media features, based on Composite Right Left-Handed transmission lines. To design the High directive antenna as a Leaky-Wave Antenna (LWA) model, we will use the artificial transmission lines to use progressive waves. To leak most of the source power the artificial transmission lines allows us to work with progressive waves. In this way, we can design an artificial transmission line through with planar technology can radiate most of the power and to achieve high directivity. While designing the LWA we will consider the dissipated power level of the antenna to measure what percentage of the total power that our design is radiating and measure efficiency our design.

## 2. Introduction to Metamaterials

The word metamaterial comes from the combination of the Greek word “meta”, which means “to go beyond” and “material” words. The theoretical properties of metamaterials were first described in the 1960s by Victor Veselago, who focused on the purely theoretical at that time concept of negative index materials. His concept became a reality in the turn of the century. To obtain the metamaterials, basically mixing up some different materials to make different structures or mixing up structures to control electromagnetic waves in any arbitrarily complex way.

Metamaterials are artificial medias can be achieved by material engineering methods. Conventional materials interact with electromagnetic radiation like light waves or radio waves based on the properties of the materials. Metamaterials interact with electromagnetic radiations but different than conventional materials the reason why, their electromagnetic properties are different. For example, in Figure 1 we can observe the light waves refractions for both Conventional and Metamaterial media, metamaterial has the negative refraction index, so the light wave refracts different than a conventional model. Also, by the controllable wave guiding property of the metamaterials it is possible to achieve the metamaterial structures for hiding objects. Invisibility cloaks are good example for metamaterial engineering to achieve unprecedented properties [1] [3].

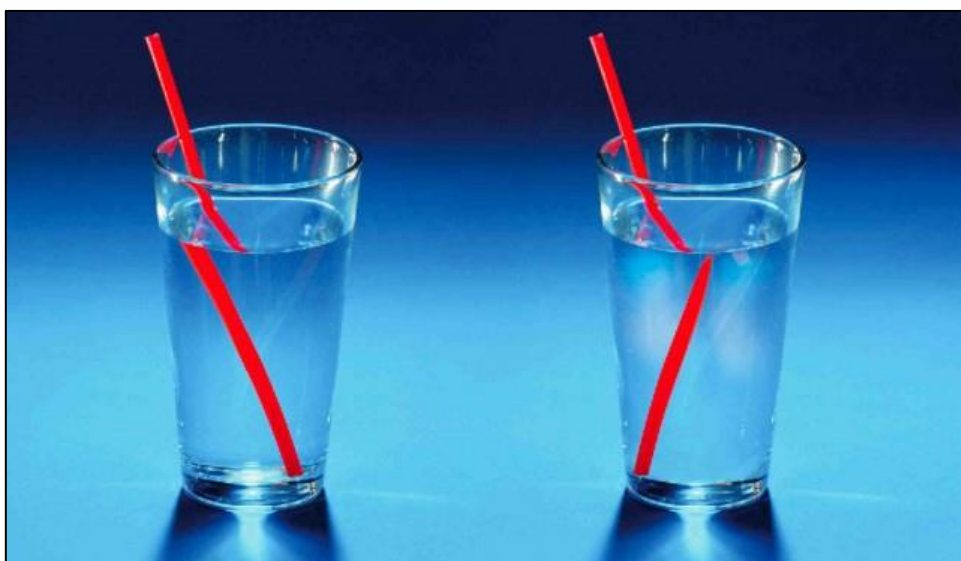


*Figure 1 The negative refractive index of Metamaterial (on the right) versus Conventional Material (on the left).*

Most metamaterials can be divided into two major classes which are Electromagnetic Crystals (EBG) and Effective media. Both types of structures are based on periodic structures. The linear size of internal inclusions in Effective media materials are much smaller than the operating wavelength. Those medias generally are accepted as homogeneous media. Therefore, Electromagnetic Crystals cannot be considered as homogeneous media. The distance between the constituent elements in Electromagnetic Crystals (EBG) structures is equal to about half the wavelength or a little more. They are usually described by Bragg reflection, which doesn't have an important role in Effective media structures, and other approaches to periodic media are used. To highlight the basic metamaterial groups for microwave applications, classification scheme shown in Figure 2 [2].

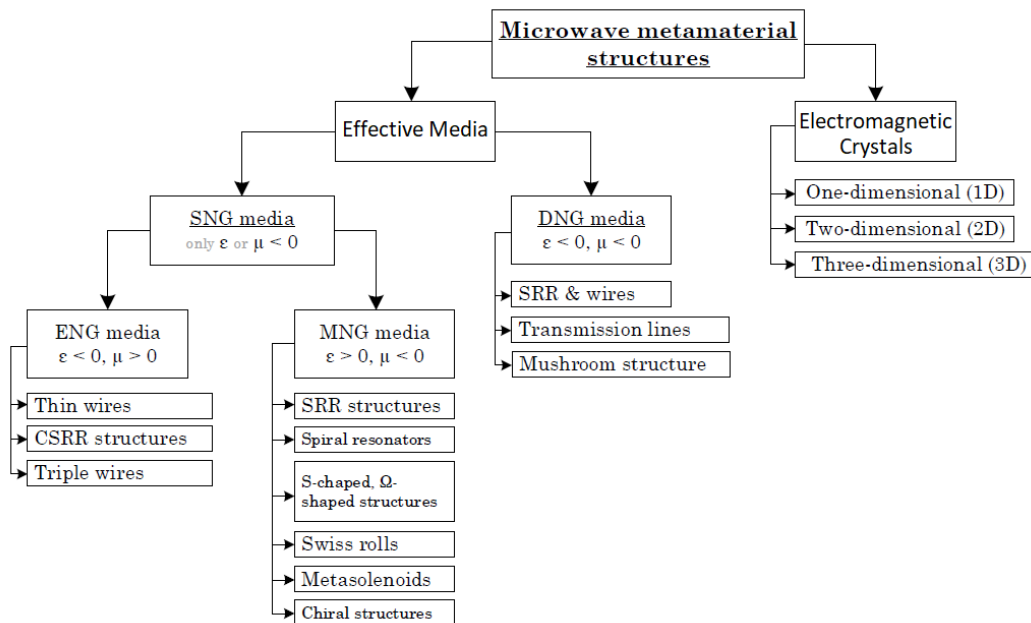


Figure 2 Classification of microwave metamaterials constructions. Figure extracted from [2]

## 2.1 Electromagnetic Crystals (EBGs)

Electromagnetic Crystals or in other words Electromagnetic Band Gaps (EBGs), are artificially fabricated periodic structures that can control the propagation of electromagnetic waves. Properly designed Electromagnetic crystals can prohibit the electromagnetic waves propagation or allow waves to propagate only along defined directions. They can also localize an electromagnetic energy in certain areas. In other

words, the permittivity of the Electromagnetic crystal varies periodically in space with a period that allows Bragg diffraction of light. These structures have a period comparable to the wavelength of the signal that propagates in the media to conduce to interference.

An advantage of the Electromagnetic Crystal is that the periodicity of permittivity changing can be changed at the choosing frequency range of the EBG material. In the EBGs, the periodicity is the result of the variation of some parameter of the media and plays a fundamental role, since this type of metamaterials can be achieved by introducing periodic disturbances to the structure. EBG based lines are periodic structures that able to inhibit signal propagation at certain frequency bands, and capacitively loaded periodic lines are not only able to filter certain frequencies, but they also exhibit a slow wave effect useful for device miniaturization. However, the controllability of the dispersion diagram and Bloch impedance of EBG-based and capacitively loaded lines is very limited, as compared to that of artificial transmission lines that mimic effective media metamaterials [7] [5].

## 2.2 Effective Media

The materials which have properties not found in nature such as the negative index of refraction ( $n$ ) are known as metamaterials. Metamaterials are artificial media that, have properties not commonly found in ordinary media. The metamaterials, which are discussed in the present section, are considered effective media because the periodicity of their elementary cells is much smaller than the wavelength at the operating frequency. Thus, it is possible to consider that the signal perceives as homogeneous free from interference. The electromagnetic properties of the metamaterials are controlled by tailoring the constitutive parameters, that is the permeability  $\mu$  and permittivity  $\epsilon$ . Depending on the material, both permeability and permittivity could have negative or positive values.

Figure 3 shows the plane divided into 4 quadrants, which represents the different medias based on the changes of the  $\mu$  and  $\epsilon$  values, where the permeability ( $\mu$ ) represents the y axis and permittivity ( $\epsilon$ ) represent the x axis. Which also shows the refraction index ( $n$ ) and its positive or negative value [2] [3].

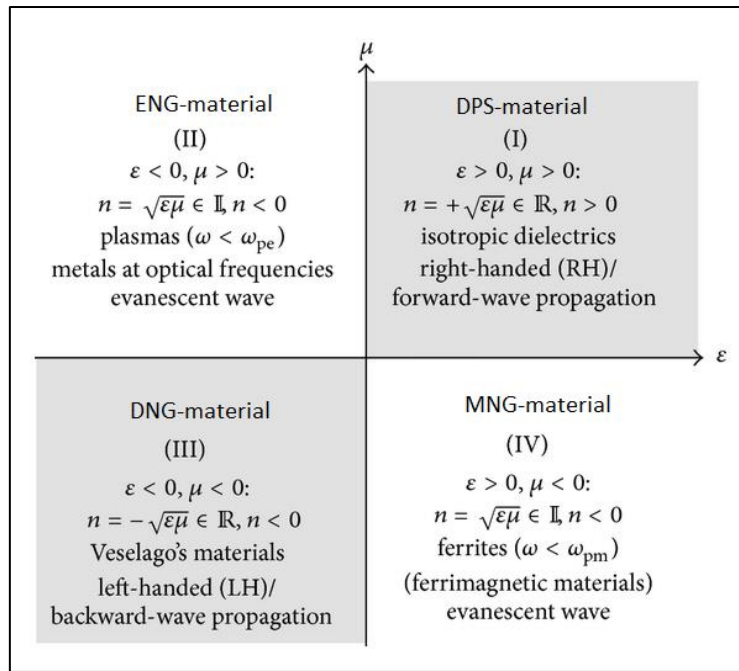


Figure 3 Classification of materials according to  $\epsilon$  and  $\mu$ . Figure edited from [3]

- Quadrant I: A medium with both permittivity & permeability greater than zero ( $\epsilon > 0, \mu > 0$ ) are called as double positive (DPS) media, they are right handed (RH) materials commonly found in nature (e.g. dielectrics). They can provide forward propagating waves and known as right handed media (RHM).
- Quadrant II: A medium with permittivity less than zero & permeability greater than zero ( $\epsilon < 0, \mu > 0$ ) are called as Epsilon negative (ENG) media, describes electric plasmas which doesn't allow wave propagation in certain frequencies.
- Quadrant III: A medium with both permittivity & permeability less than zero ( $\epsilon < 0, \mu < 0$ ) are called as Double negative (DNG) media, this quadrant represents metamaterials, they are also known as left handed media (LHM) materials. This class of materials has only been demonstrated with artificial constructs.
- Quadrant IV: A medium with both permittivity greater than zero & permeability less than zero ( $\epsilon > 0, \mu < 0$ ) are called as Mu negative (MNG) media, describes electric ferrites materials which doesn't allow wave propagation.

Thanks to effective media properties, we can fabricate artificial structures which are normally not found in nature. The left-handed media (LHM) is a kind of metamaterial, those that generate more interest in the field of microwaves, since thanks to their negative electromagnetic parameters.

The properties of effective media metamaterials and electromagnetic crystals (or EBGs) come from different principles. However, effective media metamaterials seem to offer more flexibility and controllability as compared to Electromagnetic Crystals or EBGs for the design of novel functional devices, or to improve the performance of existing ones. The research activity in the field has been progressively dominated by effective media metamaterials in the recent years, and probably this explains that most researchers consider the operation in the refraction regime as a requirement for designating an artificial periodic structure as a metamaterial. [1]

### 3. Effective Three-Dimensional Media

The first implementation of an effective left-handed media was at the end of the last century. The material had been implemented by repeating unit cells composed of metal poles and open ring resonators. The resulting media was three-dimensional and able to provide, thanks to the ring resonators, a negative effective permeability and thanks to the metal poles, negative effective permittivity.

#### 3.1 Introduction to Split Ring Resonators (SRR)

A Split Ring Resonator (SRR) is a device that naturally oscillates at certain resonant frequencies. SRR is a resonator, which consists of a periodic array of sub-wavelength structures that produce an electromagnetic response not available in nature. Those loops are made of non-magnetic materials like copper and with a gap between them. In Figure 4, a split ring resonator model is shown [5] [13].

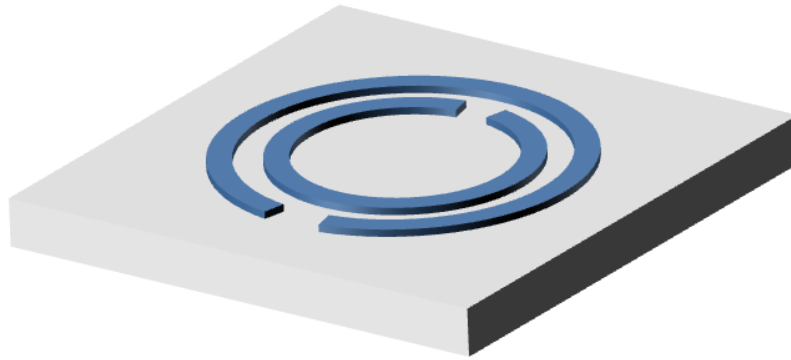


Figure 4 Split Ring Resonator (SRR). Figure edited from [8]

When a time varying magnetic field penetrates through the metallic rings and it induces an EM field by Faraday's Law of electromagnetic induction which in turn produces a rotating current. The ring produces its own magnetic field which may enhance or oppose the incident field. In Figure 5, shows SRRs considered as a resonant magnetic dipole, that can be excited by an axial magnetic field (z-direction), when we place the SRR at the bottom side of the dielectric material just behind the slot in CPW technology.

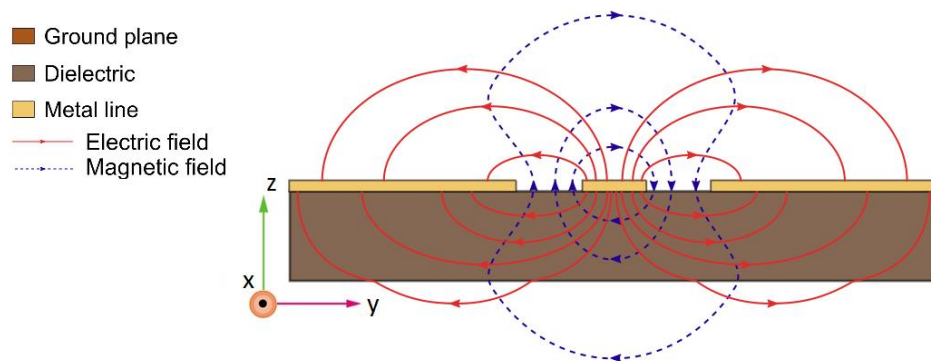


Figure 5 Electric and Magnetic fields demonstration of Coplanar Waveguide transmission line

In Figure 6, shows the variables of the SRR which are the width ( $w$ ), gap space ( $s$ ) and the radius of the ring ( $r_0$ ) and the equivalent circuit of the SRR.



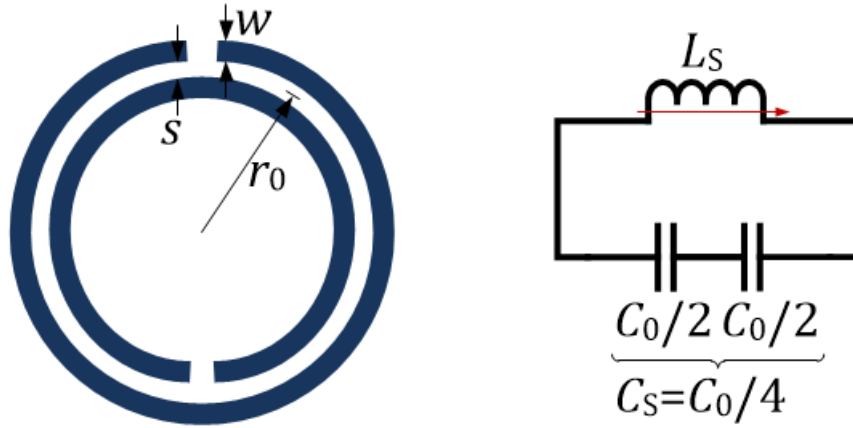


Figure 6 SRR and its Equivalent circuit Model. Figure edited from [10]

Split ring resonators can be represented by an equivalent LC circuit. The capacitance effect ( $C_S$ ) comes from the directly gaps between the split rings ( $s$ ) as an effect of parallel plate capacitor. And the inductance effect ( $L_S$ ) comes from the thickness of the rings ( $w$ ). The values of the capacitance and inductance depends on the diameter of the rings, the width of the split and the material is used. The equivalent LC circuit has a natural frequency associated with it which is given by the following formula:

$$f = \frac{1}{2\pi\sqrt{LC}} \quad (3.1)$$

When a frequency of the incident field comes near that resonant frequency, current flows in a high opposing field resulting in a low effective field. Many split ring resonators are arranged in a periodic array such that EM (Electromagnetic) waves interact with them as a homogenous media. The system has an effective natural resonant frequency which can be tuned by changing the dimensions of the rings. Thus, we can have a media having a negative permeability ( $\mu$ ) for an adjustable range of frequencies [5] [13].

## 3.2 Introduction to Complementary Split Ring Resonators (CSRR)

Complementary split ring resonators (CSRRs) are another type of media based on resonant elements. Complementary split ring resonators (CSRRs) are introduced as an alternative design which can provide a negative permittivity ( $\epsilon$ ) by means of an array [5]. According to the duality and complementarity concepts, the CSRR can be derived from the SRR structure in a simply way in Figure 7. Complementary split ring resonators (CSRRs), in planar technology can be defined as the negative image of the SRR, exhibits an electromagnetic behaviour that is the dual of the SRR. Which can be provable by achieving the negative permittivity ( $\epsilon$ ) effect instead of achieving permeability ( $\mu$ ) effect different than SRRs based media [5] [13].

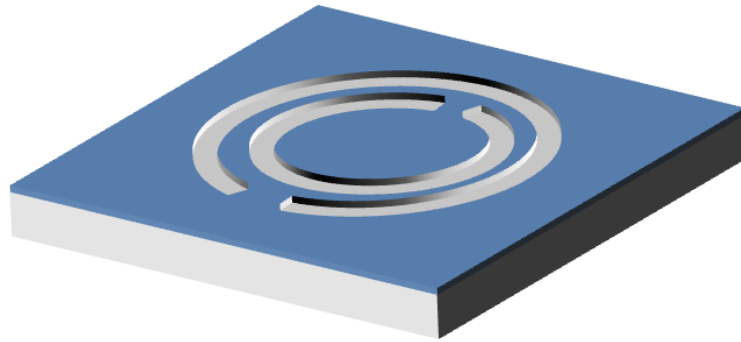


*Figure 7 Complementary split ring resonators (CSRR). [8]*

Perfectly dual behaviour is expected for the complementary shape of the SRR. We know that the SRR mainly considered as a resonant magnetic dipole that can be excited by an axial magnetic field in CPW technology which shown in Figure 5. The CSRR behaves as an electric dipole at the same resonance frequency of the SRR with same dimensions. CSRRs can be excited by an axial electric field (z-direction), where CSRRs exhibit a resonant magnetic polarizability along the x-axis in microstrip technology, see Figure 8. Also, its fundamental resonance can excite by an external magnetic field applied along the x-axis in microstrip technology. At its fundamental resonators, excitations can be achieved by placing the CSRR on the ground plane of a microstrip transmission line just behind the slot [5] [13].

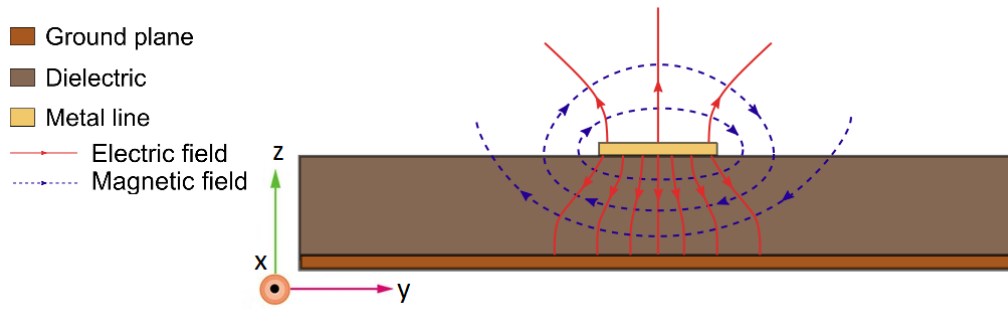


Figure 8 Electric and Magnetic fields demonstration of microstrip transmission line

Complementary Split ring resonators (CSRRs) can be represented by an equivalent LC circuit shown in Figure 9. Where  $L_c$  and  $C_c$  are the inductance and capacitance of the CSRR, respectively. For the CSRR, the capacitance  $C_c$  is achieved as the capacitance of a disk of radius ( $r_0$ ) surrounded by a metal plane. The inductance  $L_c$  is given by the parallel combination of the two inductances connecting the inner disk to the outer metallic region of the CSRR. Therefore, under such ideal conditions, the resonance frequencies of the CSRR is same as with SRR, because of duality. However, the conductor has a finite width and losses, and a substrate is needed, which means that the resonance frequencies of the metal and complementary particles are not exactly but most likely the same. Both the SRRs and the CSRRs can be used to achieve effective media, means of negative effective permeability or negative effective permittivity respectively. The fact of choosing one or the other depends on our design, the type of technology chosen for the implementation of proposed media and the way in which the chosen particle is excited [5] [13].

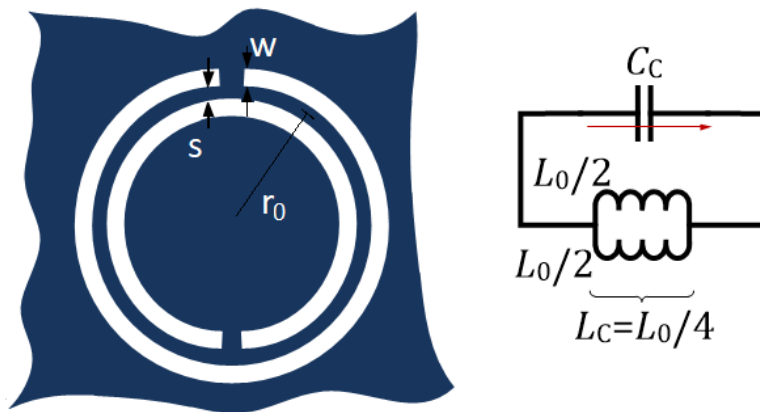


Figure 9 CSRR and its Equivalent circuit Model. Figure edited from [10]

As a result, considering the CSRR behaves like a resonant electric dipole excited axially by an electric field at its fundamental resonance frequency in Figure 8 as a microstrip technology example, for which the SRR behaves like an axial magnetic dipole as a CPW technology example, see in Figure 5.

### 3.3 Negative Effective Permeability Media (MNG)

To implement the negative permeability media (MNG) the most current design is set of conducting rings placed in array to realization of a negative permeability media for EM radiation polarized with the magnetic field parallel to the ring's axis.

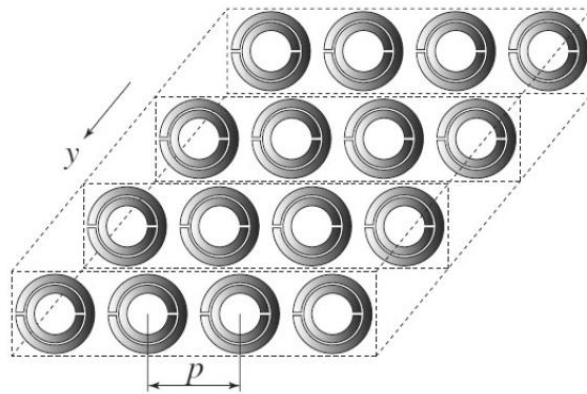


Figure 10 Artificial MNG media corresponds with array of SRRs that constitutes an effective permeability.

When a time-varying magnetic field is applied to the axial direction (y-direction), current loops are induced in the rings, and current flows from one ring to the other through the distributed edge capacitances between the rings. If both rings are very close one each other, the edge capacitance is significant, resulting in considerable coupling between both rings. Considering that the behaviour of the SRR is modelled by a parallel LC resonance showed in Figure 6, periodic array of SRRs activated by an axial magnetic field to the resonators can emulate an effective media. Certain regions of frequency, the magnetic permeability ( $\mu$ ) takes negative values, thus inhibiting the propagation of the signal. Expression for calculate the effective permeability ( $\mu$ ) can be written as follows [5]:

$$\mu_{eff} = \mu_0 \left( 1 - \frac{F \omega^2}{\omega^2 - \omega_0^2 - j\omega\Gamma} \right) \quad (3.2)$$

Where  $F$  is a geometric factor that refers to the fractional volume of the SRR with respect to the total volume of the structure, and  $\omega_0$  represents the resonance frequency of the SRR. The  $\mu_{eff}$  is plotted as a function of frequency in Figure 11 and it is obtained that the magnetic permeability is positive below the resonance frequency and negative in a certain frequency band of above the resonance frequency represent with the range of  $\omega_0 < \omega < \omega_0/(1 - F)^{1/2}$  extracted from the given formula, which shown in Figure 11 with blue shaded area [5].

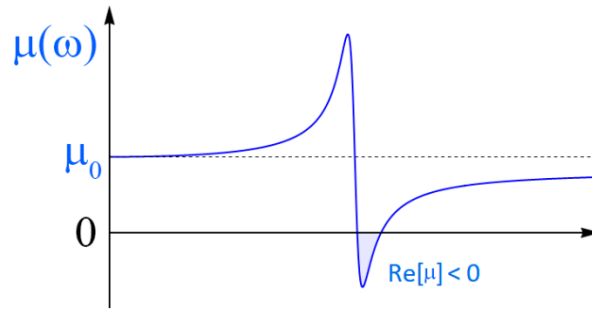


Figure 11 Effective permeability as a function of frequency. Figure edited from [12].

### 3.4 Negative Effective Permittivity Media (ENG)

When we consider a square latticed of metallic wires for incident plane waves polarized with the electric field parallel to the wires ( $z$ -direction) shown in Figure 12. The  $p$  is representing the distance between wires and  $r$  is the radius of wires. This system can be modelled by a TEM transmission line loaded with metallic posts [5].

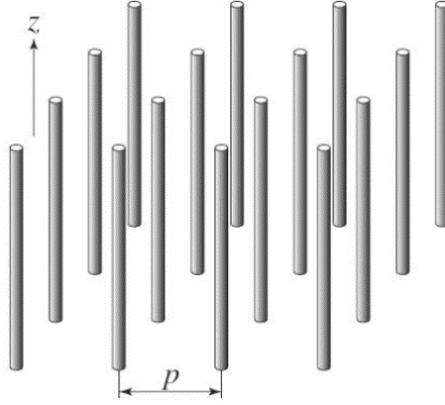


Figure 12 Artificial wire media exhibiting negative effective permittivity. Figure edited from [5].

The behaviour of structure can be demonstrated by means of plasma resonance in a metallic wire. Thus, the system of wires, for the considered polarization conditions, behaves as an ideal plasma, with plasma frequency and effective permittivity by given formulas [5]:

$$\omega_p^2 = \frac{2\pi}{\mu_0 \epsilon_0 p^2 \ln(p/r)}, \quad \epsilon_{eff} = \epsilon_0 \left( 1 - \frac{\omega_p^2}{\omega^2} \right) \quad (3.3)$$

We can observe that the electric permittivity takes negative values for frequencies lower than the plasma frequency and controlling the relationship with the distance between the wires and the radius of wires, it is possible to adjust the frequency of the plasma with the aim of the implementation media with capable of offering an  $\epsilon < 0$  to the desired frequency. By considering the current induced in the wires by the external electric field. It has also been demonstrated that a cubic mesh of metallic wires behaves as an isotropic artificial plasma for all wave polarizations and propagation directions [5].

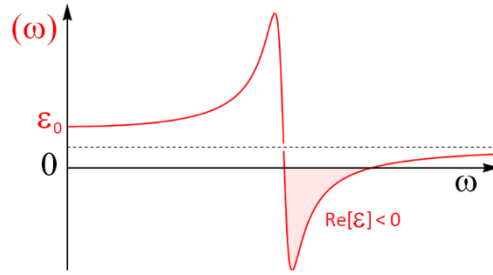


Figure 13 Effective permittivity as a function of frequency. Figure edited from [12].

The  $\epsilon_{eff}$  is plotted as a function of frequency in Figure 13 and it is obtained that the electric permittivity is positive above the plasma frequency and negative in a certain frequency band of below the plasma frequency, which shown in Figure 13 with red shaded area. The effective electric permittivity of the structure in Figure 12 in the z-direction is also same with the electric field vector axial direction also shown in Figure 13.

### 3.5 Left-Handed Media (LHM)

The Left-Handed media concept is basically to combining the properties of the both medias, ENG and MNG, and obtaining a composite structure, which presents an LHM behaviour. The first LH media is formed by a combination of the media of wires and SRRs, both to excited for a certain frequency range to achieve, simultaneously, negative values of both  $\epsilon$  and  $\mu$ . It is recalled that the media of the SRRs is excited with an axial magnetic field, in the direction of the axis of the rings, while the media of the wires is excited with an axial electric field to the wires. The structure that represents the first Left-Handed media turns out to be three-dimensional which shown in Figure 14. This fact greatly limits the possibility of applying its properties [5].



Figure 14 Effective left-handed artificial media (LHM) formed by a combination of ENG and MNG medias. Figure extracted and edited from [3].

### 3.5.1 Propagation of Waves in LH Media

The refractive index of a material is a dimensionless number that describes how fast light propagates through the material.

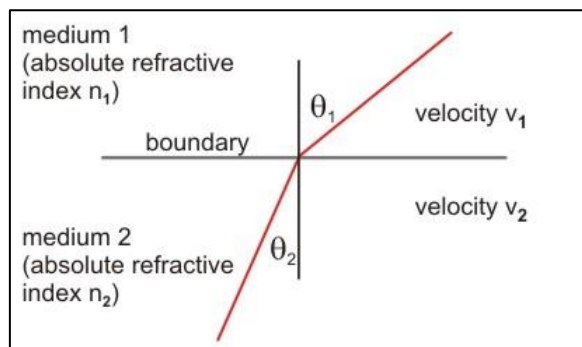


Figure 15 The refractive index of two different medias



The refractive index of media defined with the letter ( $n$ ). This variable is directly related to the propagation of an electromagnetic wave in the same media, the propagation constant of the wave  $\vec{k}$  related to the frequency and the speed of light by means of the following formula:

$$n = \sqrt{\varepsilon \cdot \mu}, \quad \vec{k} = \frac{\omega}{c} \cdot n \quad (3.4)$$

When we assume the media as a lossless media, so that  $\varepsilon$  and  $\mu$  are real numbers, simultaneous change of these electromagnetic parameters does not affect the previous equations. However, to understand what the simultaneous change of signs suggests, a study of the Maxwell equations is required, where the variables  $\varepsilon$  and  $\mu$  appear separately [5].

$$\vec{\nabla} \times \vec{E} = -j\omega\mu\vec{H} \quad (3.5)$$

$$\vec{\nabla} \times \vec{H} = j\omega\varepsilon\vec{E} \quad (3.6)$$

Considering that the waves, which propagate through this lossless media, are flat and that the propagation constant  $|\vec{k}| = \frac{2\pi}{\lambda}$ , where  $\vec{k}$  is the wave vector, so we can simplify the equations as this:

$$\vec{k} \times \vec{E} = \omega\mu\vec{H} \quad (3.7)$$

$$\vec{k} \times \vec{H} = -\omega\varepsilon\vec{E} \quad (3.8)$$

For positive permittivity and permeability values, the vectors  $\vec{E}$ ,  $\vec{H}$  and  $\vec{k}$  form are orthogonal to each other respect to the right-hand rule, while if the same values are negative, a left-handed rule would result, and the equations would be rewritten as follows [5]:

$$\vec{k} \times \vec{E} = \omega|\mu|\vec{H} \quad (3.9)$$

$$\vec{k} \times \vec{H} = -\omega|\varepsilon|\vec{E} \quad (3.10)$$

And the Poynting vector is defined by the following relationship of the electric and magnetic fields:

$$\vec{S} = \frac{1}{2} \vec{E} \times \vec{H}^* \quad (3.11)$$

The real part of the Poynting vector defines the direction of power flows and its invariant to a simultaneous change of signs of  $\epsilon$  and  $\mu$ . So, the vectors  $\vec{S}$ ,  $\vec{E}$  and  $\vec{H}$  are orthogonal and form a right-handed rule in both the RH media and the LH media. However, in right-handed media, the vectors  $\vec{\beta}$  and  $\vec{S}$  are parallel, they share direction and meaning, and in the left-handed media these vectors are anti-parallel, they have the same direction but opposite directions. In Figure 16, it shows the directions of the vectors [5].

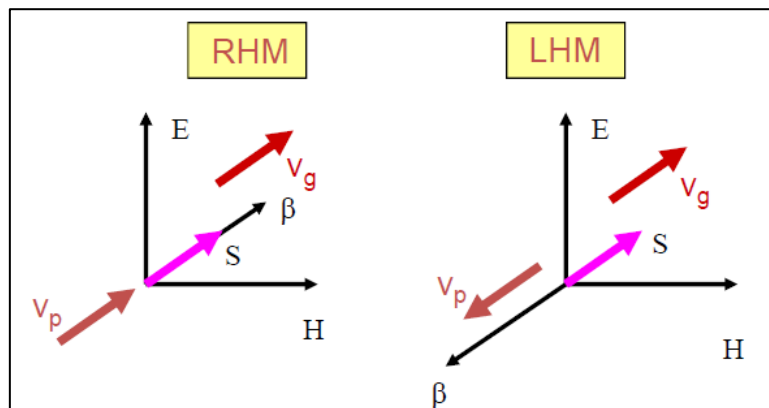


Figure 16 Directions of  $\vec{S}$ ,  $\vec{E}$ ,  $\vec{H}$ ,  $\vec{\beta}$ ,  $\vec{V}_g$  and  $\vec{V}_p$  Vectors for both RHM and LHM. Figure extracted from [14].

## 4. Metamaterial Transmission Lines

Based on the previous chapter here we will focus on the left-handed media (LHM), its implementations and applications. Metamaterial transmission lines and their implementation as a one-dimensional propagating structures mainly will take a part in this section. Regarding the synthesis of metamaterial transmission lines, most of the chapter will be mention the resonant-type approach, and where the formerly constitutive particles for the implementation of left-handed structures, with the SRRs and the dual version of the SRRs which is CSRRs are used in combination with other elements. The lumped-element equivalent circuit models were showed for left-handed media and single negative transmission lines loaded with both SRRs and CSRRs will be presented, analysed, and discussed. These models are fundamental for the design of microwave components based on SRRs and CSRRs [15].

Before we start to analyse the dual and conventional transmission lines and their propagation characteristics as a backward and forward transmission lines first. I want to mention about phase constant ( $\beta$ ) and Bloch impedance ( $Z_B$ ) concepts which will be very useful to understand the following sections and help to analysis the propagation characteristics of the transmission lines better.

### - Phase Constant ( $\beta$ ):

When we consider that the fields in the open periodic structure vary in both the longitudinal and transverse directions. The total wavenumber  $\vec{k}$  of each space harmonic given by [14]:

$$\vec{k}^2 = \vec{k}_n^2 + \vec{k}_t^2 \quad (4.1)$$

- If the  $\vec{k}_n^2 > \vec{k}^2$ , this means that the  $k_t$  is imaginary and this does not allow radiation, which is also known as a slow wave.
- If the  $\vec{k}_n^2 < \vec{k}^2$ , this means that the  $k_t$  is real and it does allow radiation, which know as a fast wave.

When the propagation constant refers to second case than we can check the radiation direction.

- If  $0 < k_n < |k|$ , is provided this means the radiation is forward
- If  $-|k| < k_n < 0$ , is provided this means the radiation is backward

In Figure 17, (a) is represents the forward wave and (b) represents the backward waves.

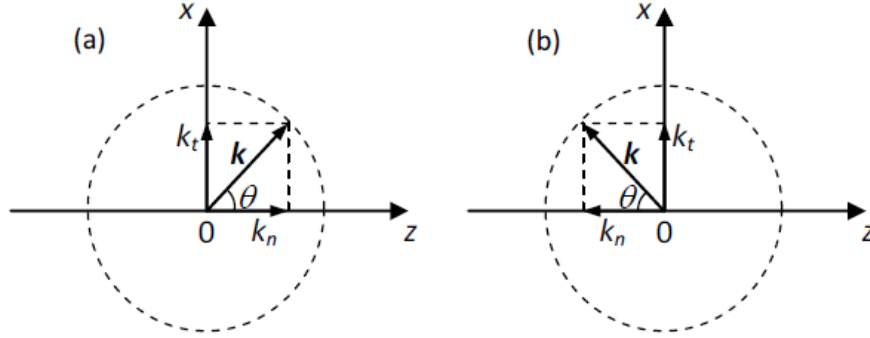


Figure 17 Generation of a forward (a) and backward (b) leaky wave in a periodic structure. Figure extracted from [14]

In Figure 17, the  $k_n$  value also represents the  $\beta$  value. It come from the boundary conditions, which refers to the components of the propagation constant ( $k$ ), which lies in the same direction with the periodic structure lies ( $z$ -direction), the phase constant of the periodic structure ( $\beta$ ) and the component of the propagation constant ( $k_n$ ) must be equal  $k_n = \beta$  [14].

#### - Bloch Impedance ( $Z_B$ )

When a unit cell circuit has a ladder-network topology, the most convenient method of analysis is by transfer matrix (ABCD matrix). When we consider the infinite TL as being composed of a cascade of identical two-port networks, we can relate the voltages and currents on either side of  $n$ -th unit cell using the transfer matrix [11],

$$\begin{bmatrix} V_n \\ I_n \end{bmatrix} = \begin{bmatrix} A & B \\ C & D \end{bmatrix} \begin{bmatrix} V_{n+1} \\ I_{n+1} \end{bmatrix} \quad (4.2)$$

where A, B, C and D are the matrix parameters for cascade of a TL section with the unit length is  $l$ .

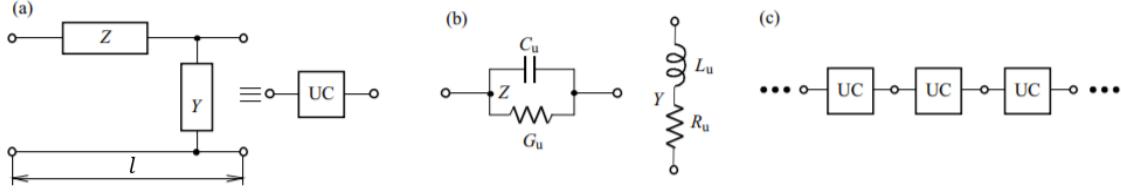


Figure 18 (a) Unit cell of TL, (b) Lumped elements of the unit cell, (c) Periodic artificial TL composed of cascading the identical unit cells (UC). Figure extracted from [11]

According to Floquet theorem, the current and voltage waves that are propagating along the periodic structure are modified after one period by a complex constant  $\gamma l$  [11]. Since the network is reciprocal  $AD - BC = 1$ , and the expression can be simplified leading to the dispersion relation given by

$$e^{\gamma l} + e^{-\gamma l} = A + D, \quad \cosh(\gamma l) = \frac{A+D}{2} \quad (4.3)$$

When the network is lossless and reciprocal, the  $\cos(\beta l) = \frac{A+D}{2}$ . When the network is lossless and Symmetric then  $A = D$  and the  $\cos(\beta l) = A$  [11] [14]. The frequency response of Bloch impedance is determined by the model discussed above. It is important to point out that the voltage and current waves defined in previous formula, are meaningful only when measured at the terminals of the unit cells. The Bloch impedance defined as the characteristic impedance of waves on the structure and so it is given by

$$Z_B = Z_0 \frac{V_{n+1}}{I_{n+1}} \quad (4.4)$$

After some algebraic manipulations the expression for the Bloch impedance in terms of the transmission matrix elements of the unit cell yields

$$Z_B^\pm = \frac{2B}{(D - A) \pm \sqrt{(A + D)^2 - 4}} \quad (4.5)$$

When the unit cell is symmetric it becomes  $A = D$  and Bloch impedance formula can simplify as in follow:

$$Z_B^\pm = \frac{B}{\sqrt{A^2 - 1}} \quad (4.6)$$

The  $\pm$  solutions correspond to the characteristic impedance for positive and negative traveling waves, respectively. For symmetrical networks these impedances are the same except for the sign and its real, but in asymmetric networks its complex value. The real part is identical for the two solutions (forward and backward travelling waves). The imaginary part has the same magnitude but different sign [11] [14].

#### 4.1 The Dual (Backward) Transmission Line Concept

The backward transmission lines can achieve by feeding the ladder network loaded with shunt inductors and series capacitors as shown in Figure 19 (a). This ladder circuit network exactly the dual model of the conventional transmission lines which is also ladder network loaded with shunt capacitors and series inductors, Figure 19 (b), that's why it's called dual transmission line [6].

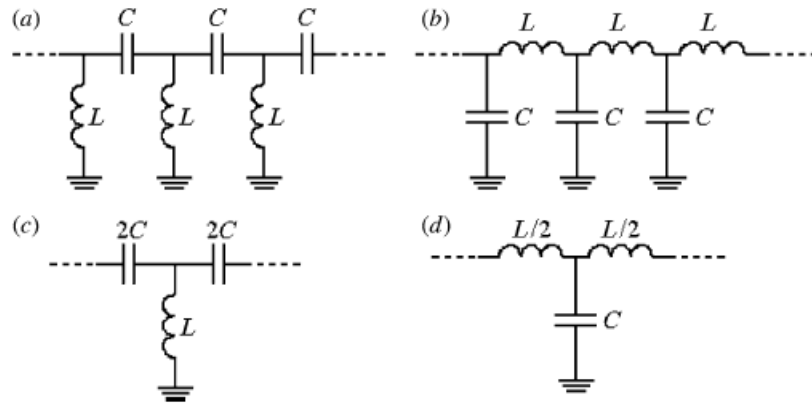


Figure 19 Equivalent circuit model of backward TL (a) and forward TL (b) respectively. The T-circuit models of the unit cell structures for backward TR (c) and forward TR (d). Figure extracted from [6].

The best way to analyse the dual transmission lines is comparing them with conventional transmission line models and mention about the differences between them, this will help the understand the propagation characteristics of both better.

The conventional transmission lines allow forward, in another word Right-Handed (RH) wave propagation, however, the dual transmission lines allow backward in another word Left-Handed (LH) wave propagation. Those wave propagation characteristics can be controlled by the values of the reactive elements which are the capacitance and inductances of the network which shown in Figure 19 [6].

The analysis of the propagation characteristics of both structures forward and backward are shown in Figure 19 can be realized from the theory of periodic structures, where it is assumed that the structure is either infinite or it is matched to the ports. From this analysis, the phase constant,  $\beta l$ , and the Bloch (characteristic) impedance,  $Z_B$ , of the transmission line can be expressed according to following formulas [6]:

$$\cos \beta l = 1 + \frac{Z_s(\omega)}{Z_p(\omega)} \quad (4.7)$$

$$Z_B = \sqrt{Z_s(\omega)[Z_s(\omega) + 2Z_p(\omega)]} \quad (4.8)$$

Where,  $Z_s$  and  $Z_p$  are the series and shunt impedances of the unit cells of the structure shown in Figure 19 (c) and (d), described by its T-circuit model, and  $l$  is the length of each unit cell. To make the formulas more specific for both backwards wave (c) and forward wave (d) unit cell structures shown in Figure 19, we can use the following expressions [6].

$$\cos(\beta_R l) = 1 - \frac{LC}{2} \omega^2 \quad \cos(\beta_L l) = 1 - \frac{1}{2LC \omega^2} \quad (4.9)$$

$$Z_{BR} = \sqrt{\frac{L}{C} \left(1 - \frac{\omega^2}{\omega_{cR}^2}\right)} \quad Z_{BL} = \sqrt{\frac{L}{C} \left(1 - \frac{\omega_{cL}^2}{\omega^2}\right)} \quad (4.10)$$

Here,  $\omega_{cR} = 2/(LC)^{1/2}$  and  $\omega_{cL} = 1/2(LC)^{1/2}$  are define the angular cut-off frequency for both forward and backward wave transmission line structures, respectively [6].

Figure 20 shows the dispersion diagrams and Bloch impedances depending on the cut-off frequency of the both conventional and dual transmission lines. In Figure 20 we can observe that the transmission is limited to cut-off frequency ranges, which means that the transmission in those structures possible under or above of those frequencies, that's also make the phase constant and the characteristic impedance to be real numbers [6].

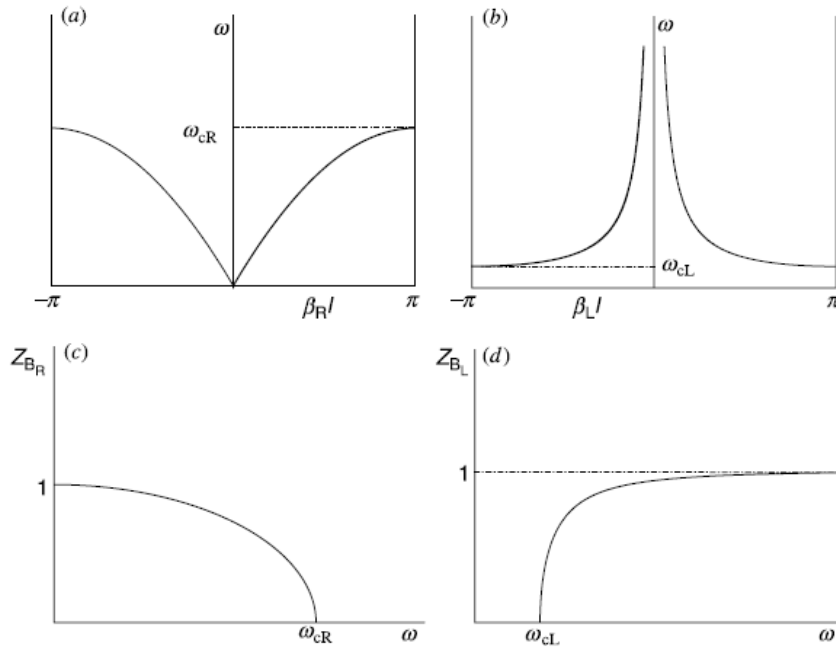


Figure 20 Dispersion diagram for forward (a) and backward (b) transmission line models and Bloch impedance with cut-off frequency for forward (c) and backward lines (d). Figure extracted from [6].

In Figure 20 (a) it models an ideal lossless forward transmission line, where dispersion is absent, in fact this circuit is only valid for frequencies satisfying  $\omega \ll \omega_{cR}$ , that is, in the long wavelength limit which corresponding to those frequencies where the wavelength for guided waves satisfies,  $\lambda_g \gg l$ . To correctly model an ideal lossless forward transmission line at higher frequencies, we need to reduce the length of the unit cell of the structure and the inductance (L) and capacitance (C) of the unit cell to increase the cut-off frequency higher. And then the model can properly describe ideal conventional transmission lines without dispersion. To do this we basically need to select the period



such that the long wavelength limit approximation holds. Under this approximation, we can use the previous defined formulas to the following well-known expressions [6]:

$$\beta_R = \omega\sqrt{LC} \quad (4.11)$$

$$Z_{BR} = \sqrt{\frac{L}{C}} \quad (4.12)$$

where L and C are the unit cell inductance and capacitance of the transmission line. We can obtain the phase and group velocities of the forward transmission line. These velocities are given by [6]:

$$v_{pR} = \frac{\omega}{\beta_R} = \frac{1}{\sqrt{LC}} \quad (4.13)$$

$$v_{gR} = \left(\frac{d\beta_R}{d\omega}\right)^{-1} = v_{pR} \quad (4.14)$$

Phase velocity ( $v_{pR}$ ) and group velocity ( $v_{gR}$ ) are both positive and constant. Which proof us both are on the same direction this is another important point to mention that on the right-handed (conventional) transmission lines group and phase velocities should be on the same direction regarding to Figure 16.

On the other hand, the backward-wave structure shown in Figure 20 (b) is dispersive even in the long wavelength limit. In left-handed transmission lines, regardless of the operating frequency within the transmission band, the structure supports backward waves. Many circuit applications of these left-handed lines are based on left-handedness, rather than on the effective media properties. The phase constant, the characteristic impedance, as well as the phase and group velocities are derived under the long wavelength limit ( $\omega \gg \omega_{cL}$ ) as you see in Figure 20 (b). And we can also obtain the following expressions like similarly in right handed structure [6]:

$$\beta_L l = -\frac{1}{\omega\sqrt{LC}} \quad (4.15)$$

$$Z_{BL} = \sqrt{\frac{L}{C}} \quad (4.16)$$

$$v_{pL} = \frac{\omega}{\beta_L} = -\omega^2 l\sqrt{LC} < 0 \quad (4.17)$$

$$v_{gL} = \left(\frac{d\beta_L}{d\omega}\right)^{-1} = \omega^2 l\sqrt{LC} > 0 \quad (4.18)$$

As we can see in the formulas the phase and group velocities have opposite signs, which is also proof that this structure supporting the backward waves regarding the schema shown in Figure 16.

The sign of  $\beta$  can be either positive or negative, this comes from the two possible directions of energy flow, namely from left to right or right to left. When we look at the conventional transmission line, the usual convention of energy flow from left to right, then the sign of the phase constant is determined by choosing that the curve that provide a positive group velocity, and this makes the  $\beta$  and  $v_g$  both positive and proof that the conventional transmission lines support forward wave transmission. However, in the dual transmission lines the energy usually flows from left to right, then the sign of the phase constant determined negative from the curve of the corresponding dispersion diagram while the group velocity is still positive. In this case, it makes the  $\beta$  negative and  $v_g$  positive and proof that the dual transmission lines support backward wave transmission [6].

## 4.2 Composite Right-Left Handed Transmission Lines (CRLH)

Implementation of CRLH transmission line, requires a host line which can be microstrip, CPW or other types. These structures can have both LH or RH wave propagation, depending on the frequency, that's why we call those structure as CRLH transmission lines. A general equivalent circuit model (unit cell) of these structures is shown in Figure 21 [5].

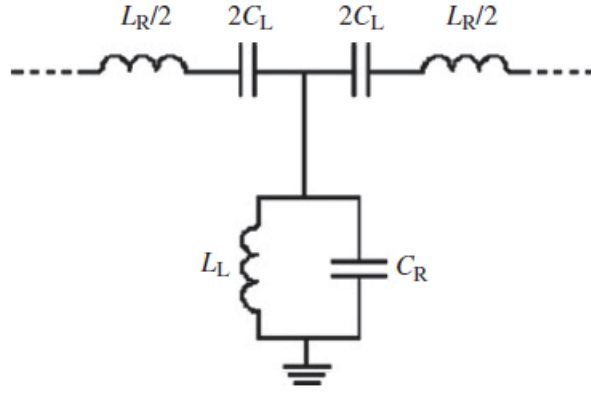


Figure 21 A unit cell of the CRLH transmission line. Figure extracted from [6]

Bloch (characteristic) impedance and the phase constant of the CRLH structures also formulized as in following:

$$\cos(\beta l) = 1 - \frac{\omega^2}{2\omega_R^2} \left(1 - \frac{\omega_s^2}{\omega^2}\right) \left(1 - \frac{\omega_p^2}{\omega^2}\right) \quad (4.19)$$

$$Z_B = \sqrt{\frac{L_R \left(1 - \frac{\omega_s^2}{\omega^2}\right)}{C_R \left(1 - \frac{\omega_p^2}{\omega^2}\right)} - \frac{L_R^2 \omega^2}{4} \left(1 - \frac{\omega_s^2}{\omega^2}\right)^2} \quad (4.20)$$

In the formula  $C_L$  and  $L_L$  are comes from the dual transmission line,  $C_R$  and  $L_R$  are comes from convention transmission line model which is also correspond the host line [5].

$$\omega_R = \frac{1}{\sqrt{L_R C_R}} \quad (4.21)$$

$$\omega_L = \frac{1}{\sqrt{L_L C_L}} \quad (4.22)$$

$$\omega_s = \frac{1}{\sqrt{L_R C_L}} \quad (4.23)$$

$$\omega_p = \frac{1}{\sqrt{L_L C_R}} \quad (4.24)$$

The frequencies above are corresponds the right-handed TR, left-handed TR, series and shunt resonance frequencies respectively shown.

In Figure 22, Bloch (characteristic) impedance and the dispersion diagram of the CRLH structures are illustrated. We can see in Figure 22 (a), there are two frequencies starts and ends the RH and LH regions, and a frequency gab between of them. We called this gap a stop bad. The lower frequency border of this gap is the end of the left-handed region ( $\omega_{G1}$ ) and upper frequency border of this gap is a start frequency of the right-handed region ( $\omega_{G2}$ ). We also call this type of CRLH models as an unbalanced CRLH because the end frequency of LH and starting frequency of RH are not same. In the left-handed region, we used the dual transmission line parameters like  $C_L$  and  $L_L$  and here the wave propagation is backward. In the right-handed region, we used the conventional transmission line parameters like  $C_R$  and  $L_R$  and here the wave propagation is forward [5].

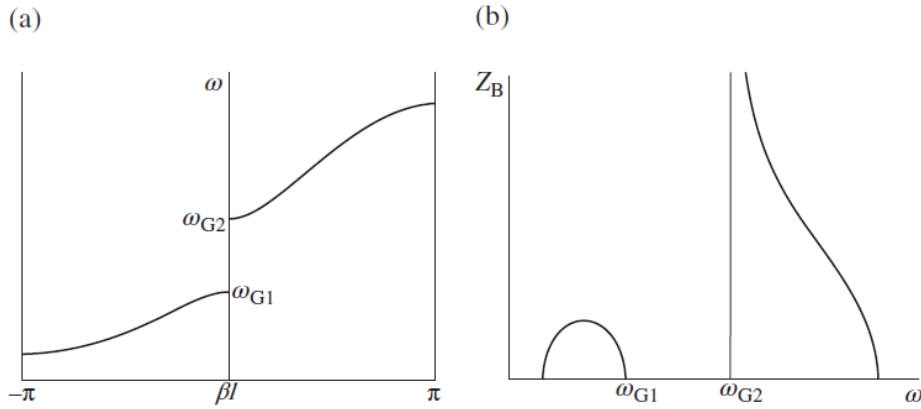


Figure 22 General dispersion diagram of Unbalanced CRLH TR (a) Bloch impedance change with frequency (b).  
Figure extracted from [5].

As we can see in Figure 22 (b), at high frequencies the CRLH transmission line tends to behave as a purely right-handed (PRH) line and in the lower limit of the first allowed band the CRLH transmission line tends to behave as a purely left-handed (PLH) transmission line. The gap frequencies limits are formalized simply by following formulas [5].

$$\omega_{G1} = \min(\omega_s, \omega_p) \quad (4.25)$$

$$\omega_{G2} = \max(\omega_s, \omega_p) \quad (4.26)$$

There is also another type of the CRLH transmission line, which called balanced CRLH transmission lines. Balanced CRLH model different than the unbalanced model the resonant frequencies of the series and shunt are the same ( $\omega_s = \omega_p = \omega_o$ ) shown in Figure 23. In this case there is not a stop band between the LH and RH frequency regions. In other words, the change between backward and forward wave behaviour is continuous. And the characteristic impedance reaches its maximum value at  $\omega_o$  which called the transition frequency [5].

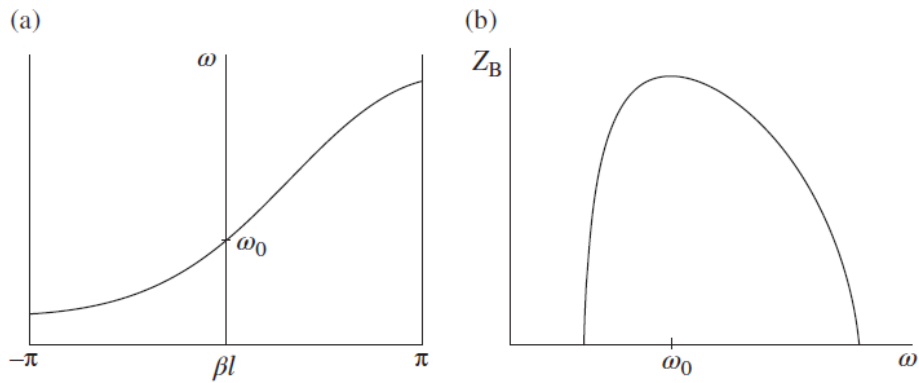


Figure 23 General dispersion diagram of Balanced CRLH TR (a) Bloch impedance change with frequency (b).  
Figure extracted from [5]

#### 4.2.1 Transmission Lines Based on Split Ring Resonators (SRRs)

The SRRs are the resonators that can be used to implement planar structure to obtain an effective media whose effective permeability ( $\mu$ ) parameters can take negative values. The transmission line, based on SRRs, was designed as an attempt to imitate the first reported LH media in planar technology. As we mentioned in the previous section the metamaterial transmission lines need a host line which can be microstrip, CPW or other types. In this case the considered host line was a CPW transmission line, loaded with pairs of SRRs and shunt connected strips. The SRRs can be excited by an axial magnetic field located at the two sides of the top layer close to central line, if we locate the SRRs far from the centre the magnetic fields can't excite the SRRs axially, see Figure 24 [5].

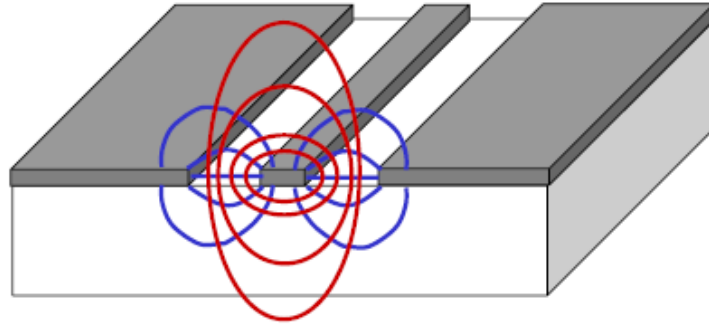


Figure 24 Distribution of the electric field lines (in blue) and magnetic field (in red) of a Coplanar Waveguide (CPW) line. Figure edited from [14].

The SRRs are etched on the back side of the substrate as shown in Figure 25 [5]. From the structure shown in Figure 24, effective constitutive parameters are providing us the behaviour of LH medias exactly same as in the CRLH model. Due to the SRRs, we can achieve MNG media, and the negative permeability ( $\mu$ ), and from the shunt-connected strips emulate the metallic wires and provides ENG media, and we can achieve the negative permittivity ( $\epsilon$ ). In Figure 25, the SRRs are placed with their centres roughly aligned with the slots of the CPW. This configuration provides the magnetic flow lines generated by the host CPW can penetrate the SRRs, and the SRRs particles can be magnetically excited [5].

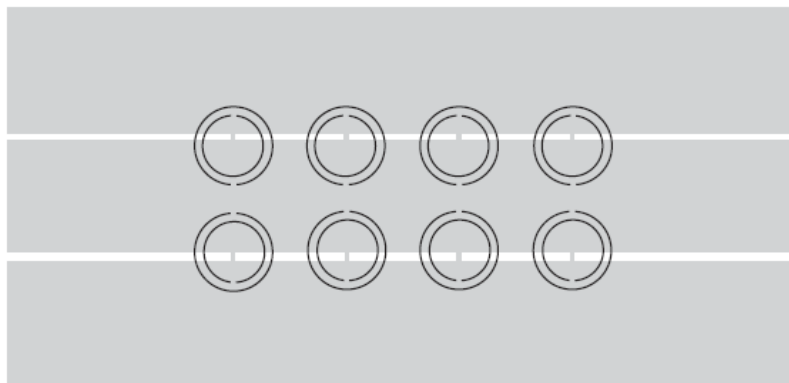


Figure 25 The layout of the CPW transmission line loaded with SRRs. Figure extracted from [13].

When we load the CPW host line only with the SRRs it behaves as a one-dimensional planar media in a lower frequency. To avoid the electric coupling between

the SRR and strips, the SRRs are etched with their slits aligned in the direction orthogonal to the line axis and the shunt strips are allocated in the symmetry plane of the SRRs [5].

To obtain the LHM behaviour from this structure it is necessary that the cut-off frequency of the strip loaded CPW should be higher than the resonant frequency of the SRR. This cut-off frequency can be controlled by the changing the dimensions of the strips of the CPW and the size of the SRRs [5].

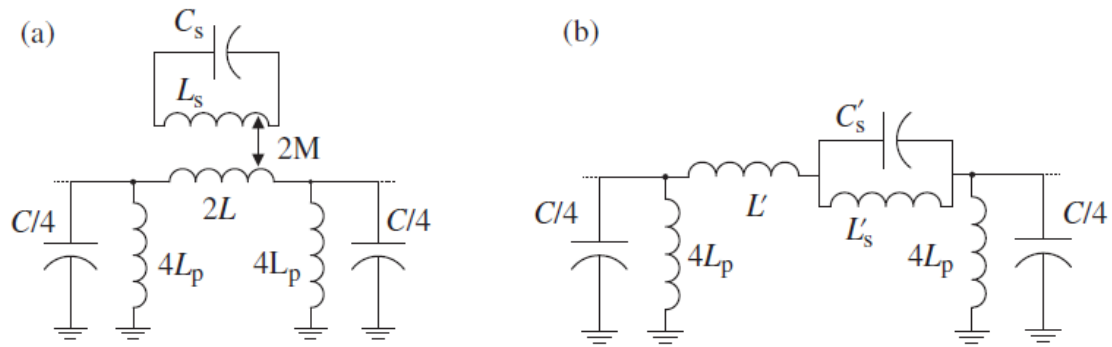


Figure 26 Equivalent circuit model for the unit cell of CPW loaded with SRR, the structure from Figure 26 (a) and the transformed version (b). Figure extracted from [5]

The previous Figure 26 shows both the discrete model of the unit cell and its simplified version of the CPW transmission line loaded with SRR.  $L$  and  $C$  account for the line inductance and capacitance comes from the CPW, and the  $C_s$  and  $L_s$  comes from the SRR model, the  $M$  is the mutual inductive coupling between the line and the SRRs, and  $L_p$  is the inductance of the shunt strips. The  $\pi$ -models of Figure 27 (a) transformed to depicted in Figure 27 (b) through the indicated transformations. The resonant frequency of the unit-cell can be calculated from the following formula [5].

$$C'_s = \frac{L_s}{4M^2\omega_0^2}, L'_s = 4M^2\omega_0^2 C_s, \quad (4.27)$$

$$L' = 2L - L'_s, \omega_0 = \frac{1}{\sqrt{L_s C_s}} = \frac{1}{\sqrt{L'_s C'_s}} \quad (4.28)$$

## 4.2.2 Transmission Lines Based on Complementary Split Ring Resonators (CSRRs)

The CSRRs are complementary particles of the SRR in a of planar transmission lines technology. As we mentioned in previous chapter that the CSRRs unit cells can be excited by axial electric field generated by the line. In this case the considered host line was a microstrip transmission line model. The CSRRs are placed with their centres roughly aligned with the slots of this microstrip line. In this way, the electric field is achieved axially to the resonators and manages to activate properly the CSRR resonators see the Figure 27 [5] [13].

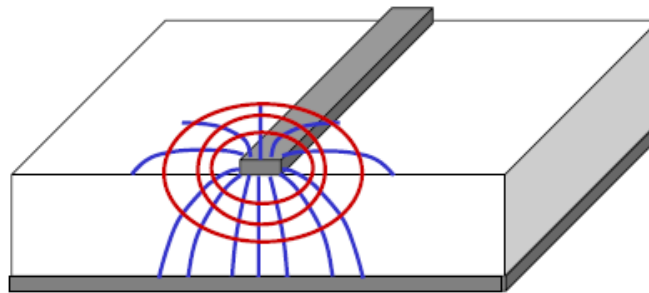


*Figure 27 Distribution of electric field lines (in blue) and magnetic field (in red) of microstrip line. Figure edited from [14].*

Here in the following Figure 28 we showed the microstrip transmission line loaded with the CSRR at the back side of the substrate. The CSRRs are resonators that can be used to implement planar structure to obtain an effective media whose effective permittivity ( $\epsilon$ ) parameters can take negative values to achieve an LH media. A microstrip line was loaded only with CSRRs, giving rise to a one-dimensional CRLH transmission line, whereas the line was loaded with CSRR and series gaps [5] [13].



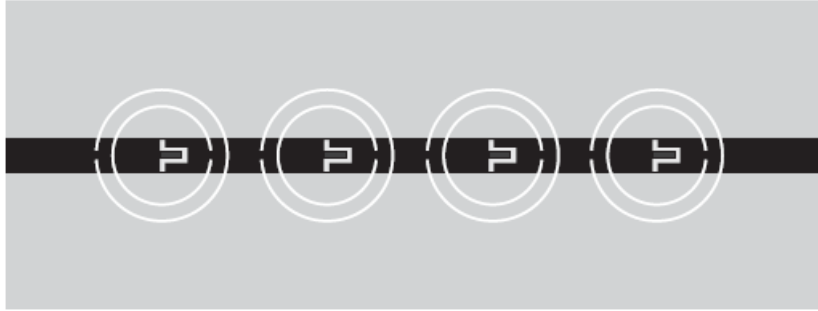


Figure 28 The layout of the microstrip transmission line loaded with CSRRs. Figure extracted from [13]

The general lumped-element equivalent circuit models of microstrip transmission line loaded with CSRRs shown in Figure 29. For the equivalent circuit model, the  $L$  and  $C$  are the per-section inductance and capacitance of the microstrip line, and  $L_c$  and  $C_c$  are comes from the CSRR model, the  $C_g$  represents the capacitance of the series gaps. We can also calculate the Bloch impedance of the unit cell from the (4.7) and (4.8) formulas.

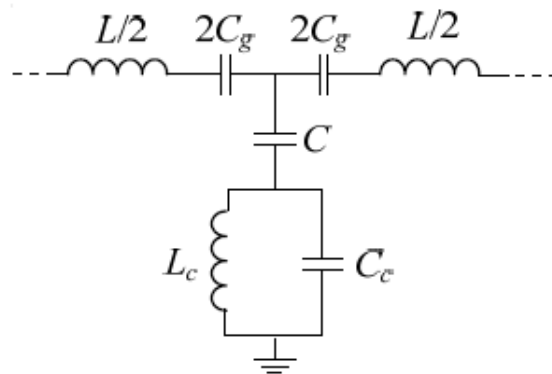


Figure 29 Equivalent circuit model for the unit cell of the microstrip line loaded with CSRR. Figure extracted from [14]

## 5. Metamaterial Based Leaky-Wave Planar Antenna Design for Bluetooth Applications

As we discussed in the previous chapter the CRLH transmission lines based on metamaterials in a planar technology, become well known and popular in last decade. While using this recent technology we can implement the Leaky-Wave Antennas (LWAs) based on metamaterials to obtain an antenna capable of radiating/leaking radio waves at

certain angle on certain frequency band. Leaky wave antennas (LWAs) based on traveling waves which are guiding the wave radiating along the structure. Uniform Leaky-Wave Antenna has a phase velocity greater than the speed of light, this type of wave radiates continuously along its length. With this type of antenna highly directive beams can be achieved at an arbitrary specified angle. As a frequency band we decide to work in Bluetooth frequency band which is 2.4 – 2.485 GHz. In this way we can make out LWA design capable of using for applications works with low frequency ranges, like for most of mobile devices.

Leaky-Wave Antennas (LWAs) based on the travelling waves can be classified into two different groups, which are uniform structures and periodic structures. Those travelling wave structures guide the wave radiations along the transmission line. In uniform LWAs, the guiding structure is uniform along the direction of propagation, and the structure supports fast waves with respect to free space, so that the complex wavenumber of the leaky mode ( $k = \beta - j\alpha$ ) has a phase constant satisfying  $0 < \beta < k$ ,  $k$  being the free space wavenumber. Uniform LWAs structures only radiate in the forward direction since ( $\beta > 0$ ), and broadside radiation is not possible in conventional uniform LWAs. However, the periodic structure used has a very small period with respect to the wavelength, so that the periodicity does not play a relevant role in the radiation phenomenon. In the periodic Leaky-Wave antennas structures, the guide structure supports slow waves in free space, ( $\beta > k$ ) where leaky wave radiation is achieved by introducing periodicity along the propagation direction. According to periodicity the fields in these periodic structures are characterized by space harmonics and the structure may radiate if the leaky wave condition ( $\beta < k$ ) satisfied for any of the space harmonics. However, in periodic LWAs, the fundamental mode does not radiate. To be able to radiate, periodic modulation of the structure produces infinite space harmonics, some of them can be fast and thus can achieve leaky-wave radiation [5].

## 5.1 Leaky-Wave Antennas Based on Metamaterial Transmission Lines

The basic operation principle of the Leaky-Wave Antenna is based on the propagation of a wave along a guided structure, with certain losses by radiation/leaking, which gradually allows the leakage of a certain fraction of the energy in the form of

coherent radiation. The first introduction of this type of Leaky-Wave antennas was in early 20th century, but with the developments in the related technologies has increased significantly in recent years. Thanks to the metamaterial and the planar technology, metamaterial transmission lines implemented to the antenna field with advantage of easy fabrication and integration. Leaky-Wave Antenna production with the planar component structures proposed planar Leaky-Wave Antenna models as well used solution [5].

The resonant antennas, where dimensions scale with the operating frequency, the length of the leaky wave structure in LWAs (uniform or periodic) is related to the antenna directivity. We know that the LWAs can achieve a high directivity with a simple structure, without need for a complicated and costly feeding network as typically used in phased arrays. Directivity increases with the length of the LWA. Under these circumstances, the radiation aperture is given by the length of the LWA, and hence a high directivity is obtained for long LWA structures. Theoretically, such scanning can contain the radiation directions between back-fire and end-fire, passing through the radiation in the broadside direction, see Figure 30 [5].

Under the condition of continuity of the interface that separates the metamaterial media from the other media that surrounds it (in most case the media is air). As we explained in the previous chapter (Chapter 4)  $k_x = \beta$  with respect to boundary conditions, where  $k_x$  is the projection of the longitudinal component of  $k_0$ . The  $k_y$  is the projection of the transversal component of  $k_0$ , and the following relationship is obtained.

$$k_0^2 = k_x^2 + k_y^2 = \beta^2 + k_y^2 \quad (5.1)$$

Considering the previous equation, it's possible to deduce that for the values of  $\beta < k_0$ ,  $k_y$  belongs to the set of real numbers ( $k_y \in \mathbb{R}$ ) so that the radiation can occur. From the equation of  $V_p = \omega/k_0$ , which expresses the relationship between the frequency, the phase constant and the phase velocity ( $vp$ ). The radiation occurs to the air, where the phase velocity is the speed of light ( $c$ ) then we can modify the formula in (5.2) [18].

$$c = \frac{\omega}{k_0} \quad (5.2)$$

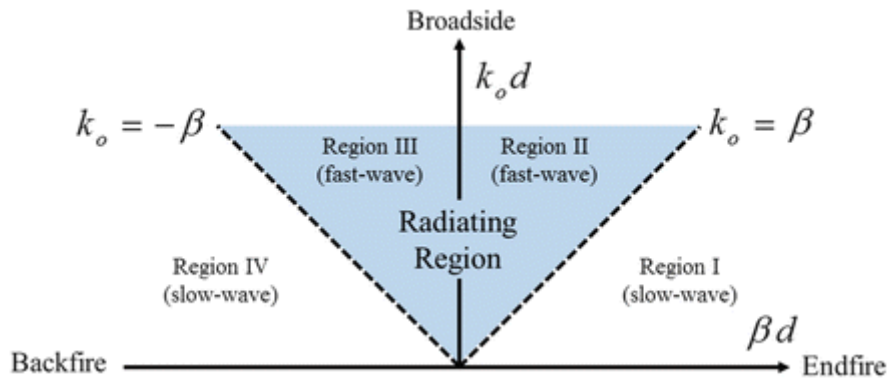


Figure 30 Dispersion Diagram of LWA with the possible directions of radiations. Figure extracted from [16].

As previously commented, the reason for the growing popularity of LWAs based on metamaterial lines is because the LWA antennas can perform a spatial sweep of the main radiation beam on a certain frequency, which can be controllable with the changing of the parameters of the antenna [16] [17].

In Figure 31 the radiation of the desired structure is showed. The shown design, starting from a metamaterial (artificial media without losses) that can vary from controlled way the phase constant of the signal (or the wave number,  $\beta$ ) that propagates in its interior. The Bloch impedance and the wave number of the signal propagating in the metamaterial ( $\beta$ ), can be controlled by an appropriate design of the structure [17].

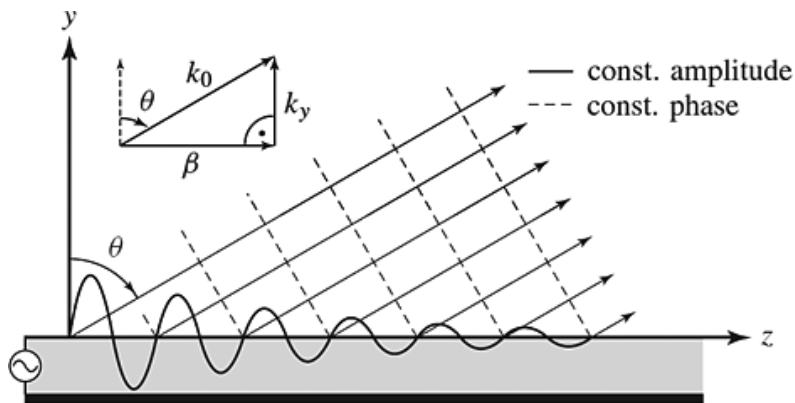


Figure 31 Typical metamaterial structure without losses shown. The signal travels inside the metamaterial has a wave number  $\beta$  while the signal radiated to the air has a wave number  $k_0$ . Figure extracted from [17].

We know that the phase constant can take both positive or negative values, and when we compare previous formula with dispersion diagram shown in Figure 30, its

proofs us the slope of the formula limits the cone of light, and its referees the fast waves, which limited with the values of  $\beta$  where the radiation is existing. For the frequencies in which the radiation is allowed shown in Figure 31, the angle that on the direction of radiation occurs can calculate with the following expression.

$$\theta = \arcsin\left(\frac{\beta \cdot c}{2\pi f}\right) \quad (5.3)$$

LWAs can be implemented by means of balanced CRLH transmission lines. Balanced CRLH lines are periodic structures by nature and balanced CRLH-based LWAs radiate from the fundamental ( $n = 0$ ) space harmonic, and essentially, they behave as uniform leaky wave structures in the sense that they are homogeneous for one-dimensional media. We can consider the CRLH-based LWAs are belong to the uniform LWAs category even though they are structurally periodic ( $l \ll \lambda_g$ ).

According to the general dispersion diagram of a balanced CRLH transmission line shown in Figure 32, there are regions where the dispersion curve lies in the fast wave region which is exactly we need to design the LWAs. The balance CRLH models is not strictly necessary.

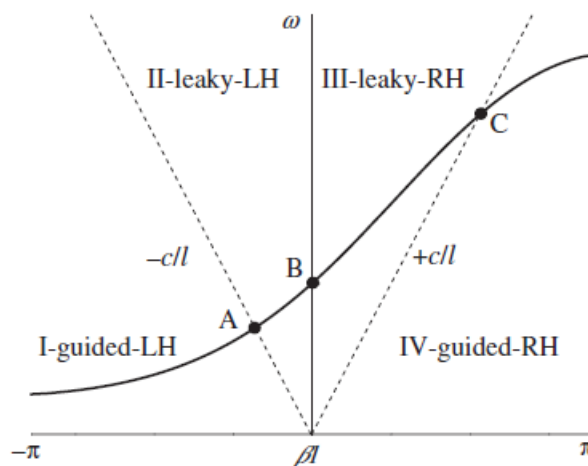


Figure 32 General dispersion diagram of a balanced CRLH transmission line and 4 main regions. Figure extracted from [5]

However, balancing the line it's providing to achieve continuous frequency scanning from backward to forward directions, including broadside radiation at the transition frequency, in other word when we use balanced model we will achieve radiation without any stop bands. Thus, balanced CRLH LWAs radiate from the fundamental mode and exhibit back-fire to end-fire capability. This is an important feature of CRLH LWAs, which is not achievable with their conventional uniform or periodic counterparts. The fact that CRLH LWAs operate at the fundamental mode is important since the feeding structures do not need to be complex, a simple transmission line is sufficing [5].

The phase and attenuation constants of the balanced CRLH structures, and the radiation patterns are different at each frequency, in the shown Figure 32. When we talk about general balanced CRLH models over the dispersion diagrams as shown in Figure 32, the LH and RH guided-wave regions are shown as I (below the frequency A) and IV (above the frequency C) respectively. The region limited with frequencies between A and B is the Region II, which is the backward radiated region (with  $|\beta| < k_0$  and  $\beta < 0$ ), and the region limited with frequencies between B and C is the region III, which is the forward radiated region (with  $|\beta| < k_0$  and  $\beta > 0$ ).

Efficient leaky wave radiation can be achieved by loading a slot line with SRRs and shunt inductive strips. With such a structure, it is possible to scan the radiation angle with frequency by balancing the line. The design of the structure starts by conceiving a balanced SRR/strip-loaded CPW with sufficiently distant slots (wide central strip) to minimize the field coupling between the slots. Balanced SRR/strip-loaded CPW with the transition frequency at  $f_0 = 2.5$  GHz was showed in Figure 33 [19].

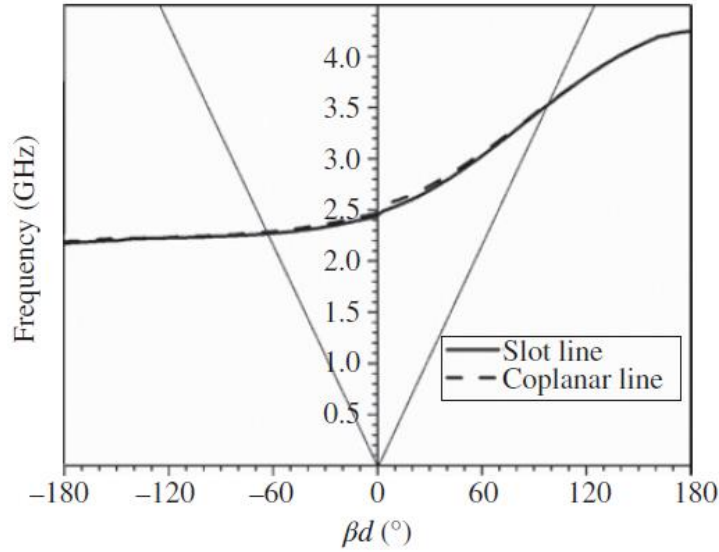


Figure 33 Dispersion diagram of the SRR loaded CPW unit cell. Figure extracted from [19].

The analysis of a single unit cell is inaccurate for the determination of the attenuation constant  $\alpha$  of leaky periodic structures. This is due to mutual coupling and edge effects. However, as the number of the considered unit cells increases, edge effects become less significant and the obtained attenuation constant is more accurate [19].

In Figure 34 we showed the shape of a unit cell. To determine the required number of unit cells ( $N$ ), the attenuation constant was computed by simulating an  $N$ -element two-port structure, using the ADC Momentum (Agilent Momentum Commercial) software. While simulations we need to aim the 90 % of the power dissipated before reaching the antenna load, until reaching this value of 90 % dissipated power we will increase the numbers of unit cells ( $N$ ), we will mention this in the proposed structure section more deeply.



Figure 34 A unit cell of CRLH transmission line. Figure extracted and edited from [19].

The angle of the maximum beam  $\theta$  as a function of frequency is also illustrated in Figure 35. The measured backward to forward scanning range is from  $-50^\circ$  to  $+60^\circ$ . The simulated and measured normalized radiation patterns are shown in Figure 35. As we can see in figure, backward, broadside and forward leaky wave radiation is obtained as frequency increases from the LH to the RH frequency bands respectively, also we can observe the radiated beam and its directivity [19].

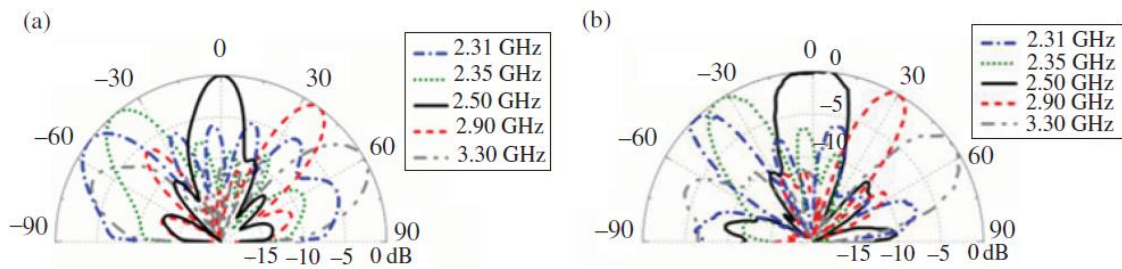


Figure 35 The simulated a) and measured normalized b) radiation patterns of the designed CRLH TR in different frequencies. Figure extracted from [19].

## 5.2 The Bluetooth Technology

Bluetooth is a wireless technology standard used to transfer data between different electronic devices. A Bluetooth technology is a high speed low powered wireless technology link that is designed to connect phones or other portable equipment together. It is a specification for the use of low power radio frequencies to link phones, computers and other network devices over short distance without wires. Wireless signals transmitted with Bluetooth cover short distances, typically up to 10 meters (30 feet).

It is achieved by embedded low cost transceivers into the devices. It supports on the frequency band of 2.4 GHz to 2.485 GHz and can support up to 721KBps along with three voice channels. This frequency band has been set aside by international agreement for the use of industrial, scientific and medical devices (ISM). In our project we decide to work in the Bluetooth frequency bands just to make our design available for the mobile devices. However, the LWA based on metamaterials technology can also support higher frequency bands like wireless frequency, it's just depended on your desires to design your LWA at any frequency.



### 5.3 Proposed Structure

In this section we will design an LWA to operate at Bluetooth frequency. To design proposed LWA, we will use microstrip technology which is loaded with CSRR resonators etched on the back side of the substrate, with this we aim to achieve LH behaviour. For the frequency of operation. We want to fit the antenna in the Bluetooth frequency band which is between 2.400 GHz to 2.485 GHz. Specifically, we want to design the antenna at 2.440 GHz. CSRR is the ideal resonator while using with planar microstrip technology. The reason is, we know from the previous caper that, there is a high electrical coupling between the microstrip host line and the CSRR rings, when they are located at the ground plane.

As we explained previously, coupling of CSRRs to microstrip transmission lines loaded with series gaps on the host line produces an effective media with LH behaviour at the corresponding frequency. Considering this property, we want to design a metamaterial structure that radiates the waves at specifically at  $\theta = -45^\circ$  with the impedance  $Z_B = 50 \Omega$ . Considering that when we want to achieve LH behaviour out  $\beta l$  should be negative and when we want to achieve RH behavior the  $\beta l$  should be positive regarding to Figure 30. Since we decided the desired radiation angle, we can calculate phase constant ( $\beta$ ) and the length of the unit cell ( $l$ ) from the following formulas. Considering that the length of the unit cell must be much smaller than the wavelength ( $l = \lambda_g/10$ ) to ensure that the structure behaves as an effective medium and the wavelength at 2.44 GHz is equal to  $\lambda_0 = 0.125$ .

$$\beta = \frac{2\pi}{\lambda_g} \rightarrow \beta l = \frac{2\pi}{\lambda_g} \cdot \frac{\lambda_g}{10} = \frac{\pi}{5} = 36^\circ \quad (5.4)$$

$$\theta = \frac{\pi}{4} \rightarrow \theta = \arcsin\left(\frac{\beta \cdot c}{2\pi f}\right) \rightarrow \beta = \frac{2\pi}{\lambda_0} \sin\left(\frac{\pi}{4}\right) = \frac{2\pi}{\sqrt{2}\lambda} \quad (5.5)$$

$$\beta l = \frac{\pi}{5} \rightarrow l = \frac{\sqrt{2}\lambda_0}{2\pi} \cdot \frac{\pi}{5} = 17.7 \text{ mm} \quad (5.6)$$

After calculating the required parameters, we can start designing the unit cell. To design the unit cell of the LWA, it is convenient to know the circuit equivalent model of corresponding unit cell. This information will allow to establish a relationship between the circuit elements and the geometric parameters of the unit cell structure. When we adjust dimensions of the unit cell at the desired frequency, we can obtain the Bloch impedance and phase constant values according to formulas (4.7) and (4.8).

In our case, the equivalent circuit model for the LWA based on CRLH loaded with CSRRs shown in Figure 36.

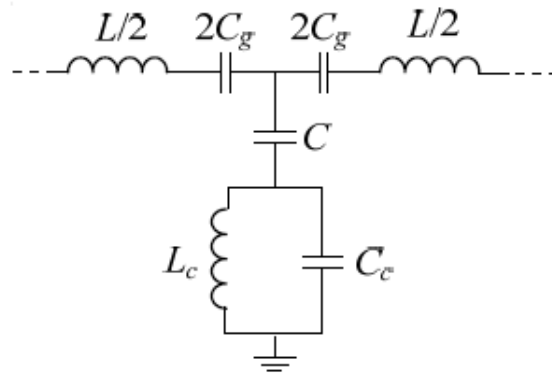


Figure 36 Equivalent circuit model for the unit cell of the microstrip line loaded with CSRR. Figure extracted from [14].

As we explained in the previous chapter (4.2.2), the microstrip transmission line loaded with CSRRs is based on the CRLH transmission lines. When we need to analyse the frequency behaviours the dispersion diagram of the CRLH transmission lines we have two option of dispersion diagrams which are the balanced and unbalanced cases. Since we know the only difference between two model is there is a frequency gap, which support an evanescent mode (no radiation allowed) because there is no continuous transition from the LH mode to the RH mode of the line. We know that our model allows us to deal with unbalanced CRLH dispersion diagram model, since the balanced case is very hard to achieve in practice. For the unbalanced case we have the dispersion diagram in Figure 37, where we can observe the frequency gap which an evanescent mode occurs.

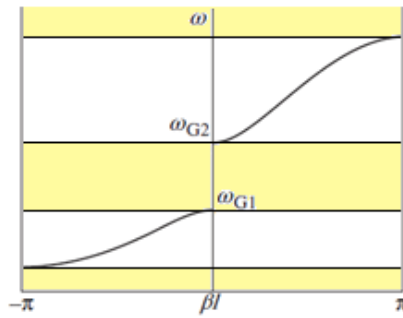


Figure 37 Dispersion diagram of Unbalanced CRLH TR. Figure extracted and edited from [5].

When we examine the diagram, we can see that at low frequencies, below the LH band, high frequencies above the RH band and the band in between with LH and RH regimes (shown with lower yellow area), there are an evanescent mode (no radiation allowed). The reason of those bands doesn't allow radiation is because of the increasing frequency level is directly affecting each of components on the unit cell circuit model their behaviours. We can explain the transition between each mode more detailed. We can see from the dispersion diagram shown in the Figure 37, there are 3 different modes occurs while the frequency change.

The first mode is evanescent mode, at the lower frequencies, the resonators of the series branch have a capacitive behaviour, while the parallel branch is modelled by a resonator ( $L_c C$ ) series, and this in turn behaves capacitively and the resulting model makes it impossible for to be any transmission between the ports.

When we increase the frequency, the behaviour varies so that the branch in derivation now behaves inductively, and adjusted resulting model defines as a dual transmission line, which formed by series capacitance and parallel inductance and achieves to LH behaviour (LH mode). This behaviour is induced by the resonance of the resonator formed by the capacity of the host line ( $C$ ) and the coil ( $L_c$ ) of the CSRR.

Further on, the CSRR resonates giving rise to the second evanescent mode where both the resonators of the series branch and the branch behave as a capacity, thus cancelling the existing transmission between the ports of the line and ending the band where There is backward radiation.

After the previous evanescent mode, the RH behaviour (RH mode) begins where the forward radiation starts. The resonance of the series resonator formed by the gap capacity ( $C_g$ ) and the inductance of the line itself (L). The behaviour varies causing the resulting model to approach series inductance and parallel capacitance. In Figure 38 we showed the transition between the modes.

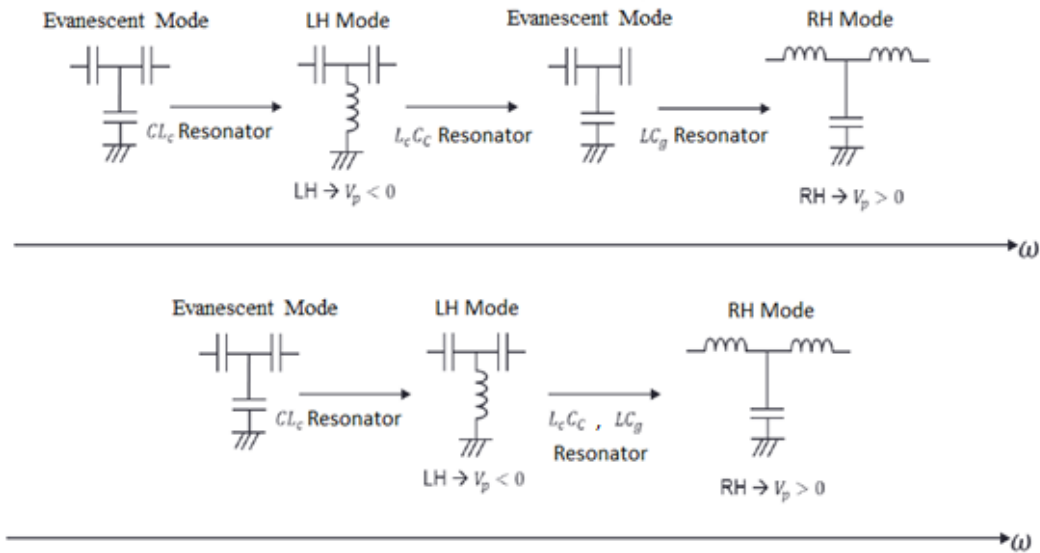


Figure 38 Frequency analysis of an LWA based on an unbalanced CRLH (on the top) and balanced CRLH (on the bottom) TR loaded with CSRR. Figure extracted and edited from [18].

The most important point, we can only achieve the corresponding behaviors when the length of the unit cell is much smaller than the wavelength, the Bloch impedance of the unit cell must be adapted to the ports. Since, together with the variation of the phase constant and Bloch impedance determines the behavior of the LWA [18].

## 5.4 Simulations and Experimental Results

After the analysis of the proposed structure that we will design, now we can start the simulations of the LWA. To designing and simulating the LWA we will use the ADC Momentum electromagnetic simulation software. First, we should start designing with the substrate of the microstrip transmission line. In Figure 39, we showed the correct substrate design for our structure. 2 layers and in between of the layer we used

Rogers\_RO4003 material. On the top layer cond is represents the microstrip host line and at the bottom layer cond2 represents the CSRR as slot conductor. We listed the important variables of the designed substrate below:

- $\epsilon_r = 3.55$
- $h = 0.508 \text{ mm}$  (conductor layer)

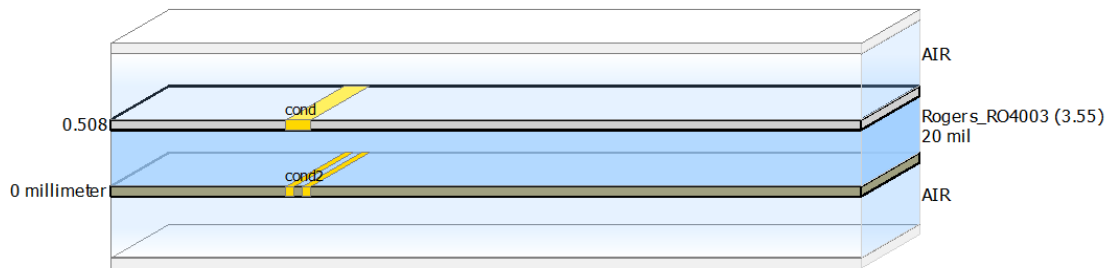


Figure 39 Substrate design of the microstrip transmission line loaded with CSRR.

Once we designed the correct configuration of the substrate, we can start with the designing layout of the unit cell. Considering the previously calculated unit cell length while using the Momentum electromagnetic simulator software, we designed the first LH unit cell as in Figure 40.

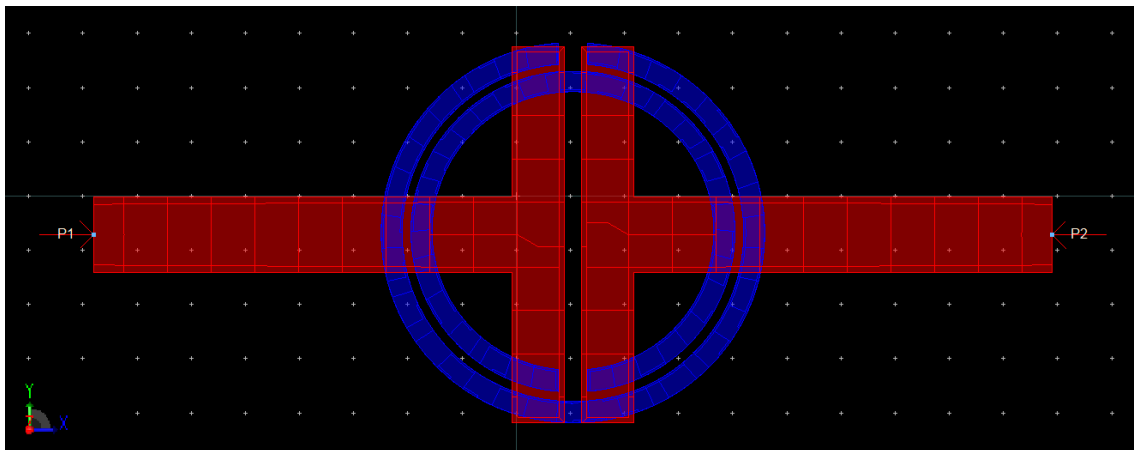


Figure 40 LH Unit cell design layout.

The layout of the LH unit cell showed in Figure 40, where the dimensions to design the proposed LH unit cell detailly listed below:

- Total length of the unit cell: 17.7mm.
- The width of unit cell: 1.4 mm.
- The gap in between of microstrip line: 0.322 mm.
- Vertical length of the capacitive line strip: 6.93 mm.
- The width of the capacitive line strip: 0.96 mm.
- External ring radius: 3.46 mm.
- Separation gap between rings: 0.17 mm.
- Width of each ring: 0.4 mm.
- Gap of each ring: 0.54 mm.
- Internal ring radius: 2.64 mm.

We should underline that the line is loaded with a  $50\Omega$  ports at each end of the line. Once the unit cell has been simulated the results in Figure 41 is obtained. The first thing we can see is the graphs that  $S_{11}$  and  $S_{22}$ , also  $S_{12}$  and  $S_{21}$  has same plots. This means that the transmission from port 1 to port 2 and the transmission from port 2 to port 1 are the same. Since we know that, when  $S_{12}$  and  $S_{21}$  are identical to each other this is proofs that our design is reciprocal. As we know, the unit cell structure is symmetric vertically centered from the rings, so the parameters  $S_{11}$  and  $S_{22}$  are identical to each other. Other important point that we can observe from Figure 41 is very good adaptation at our desired frequency which is around 2.44 GHz. This indicates that the Bloch impedance is very close to the desired value which is  $50\Omega$ .

### Discrete Frequencies vs. Fitted (AFS or Linear)

Adaptively Fitted Points      Discrete Frequency Points

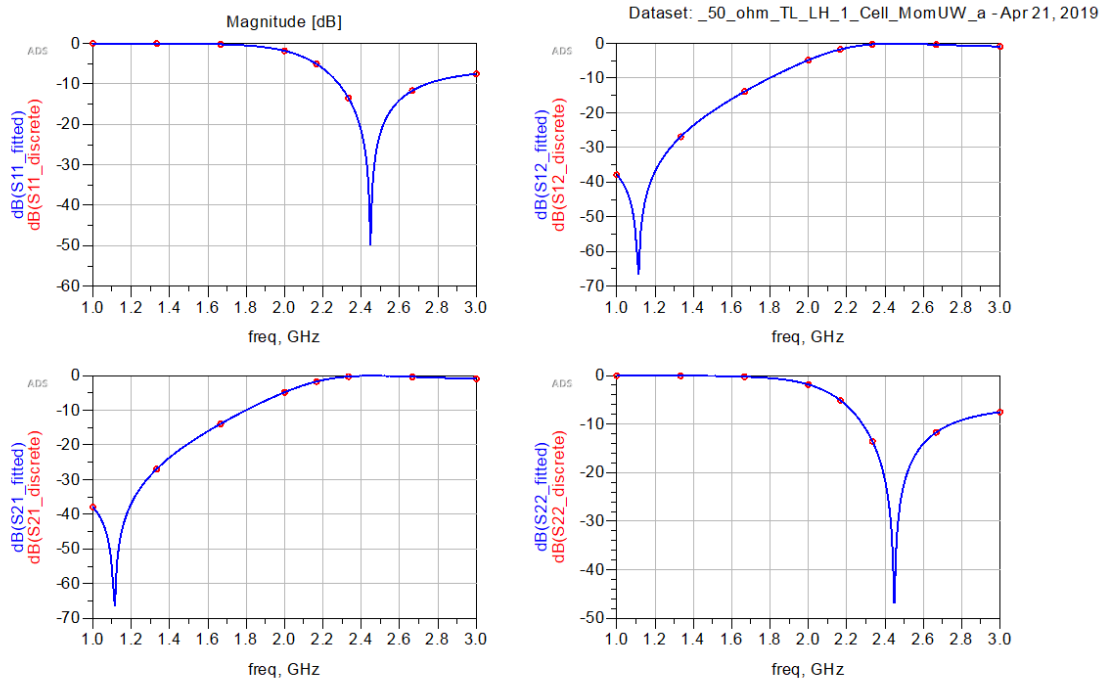


Figure 41 S-parameters of the LH unit cell

To analyse the unit cell characteristics, we need to define some equations which allow us to achieve  $\beta l$  and the Bloch impedance of the unit cell as a function of frequency, see Figure 42.

$$\begin{aligned} \text{Eqn } \text{Mat} &= \text{stoabcd}(S, \text{PORTZ}(1)) \\ \text{Eqn } A &= \text{Mat}(1,1) \\ \text{Eqn } B &= \text{Mat}(1,2) \\ \text{Eqn } C &= \text{Mat}(2,1) \\ \text{Eqn } D &= \text{Mat}(2,2) \\ \text{Eqn } ZB &= (B*1)/(((A**2)-1)**0.5) \\ \text{Eqn } bl &= \text{mag}(\text{real}(\text{acos}(A)*360)/(2*PI))) \\ \text{Eqn } bl2 &= \text{mag}(\text{imag}(\text{acos}(A)*360)/(2*PI))) \end{aligned}$$

Figure 42 Equations for to achieve the unit cell characteristic parameters

Once we de defined the equations, for the next step, we should add following 4 graphs which are important to analysis the unit cell characteristics. Those graphs are S11 and S21 graphs, to see reflection and transmission coefficients respectively,  $\beta l$  and  $\beta l_2$  graph to see the  $\beta l$  value related with radiation angle and ZB graph which shows us the Bloch impedance as a function of frequency, see Figure 43.

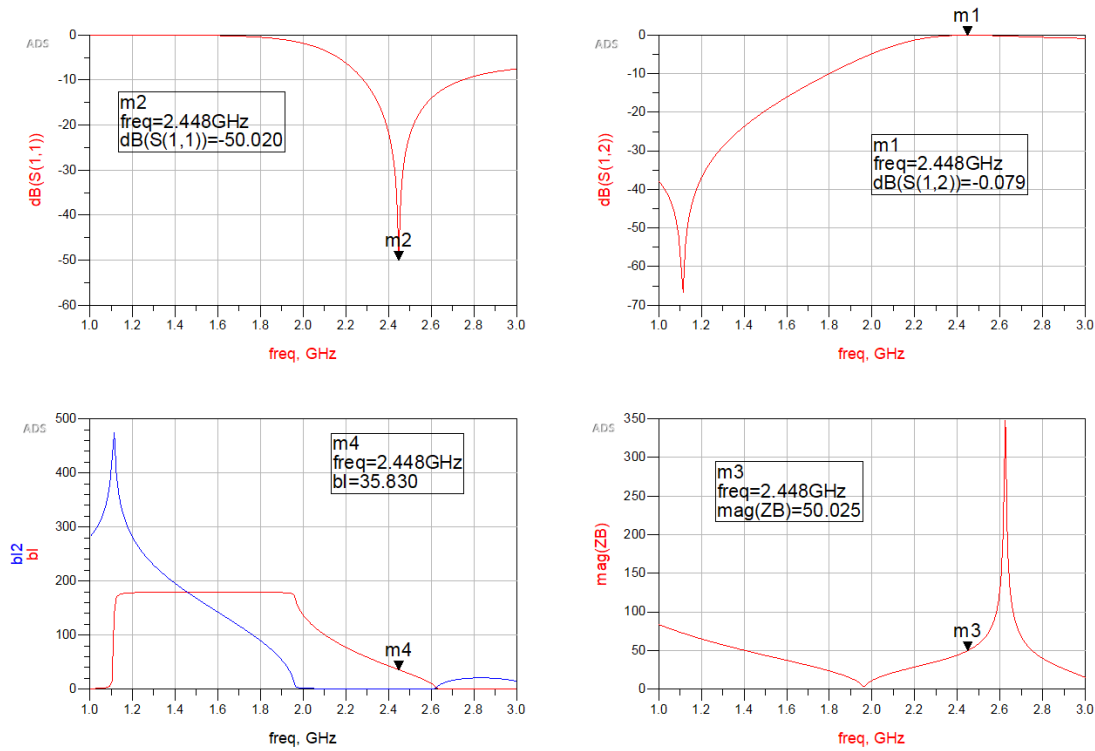


Figure 43 LH unit cell characteristic parameters

When we take a close look at each graph in Figure 43, we can mention that the S11 and S21 parameters have a good match around the desired frequency (2.44 GHz). This means that our design has less reflection (S11) and high transmission (S21) at the desired frequency, which is good in terms of transmission.  $\beta l$  is plotted as a function of frequency to see if the radiation is on the correct direction. As we calculated before, to achieve a radiation at  $\theta = 45^\circ$ , we need to achieve  $\beta l = 36$ , so that the backward radiation will occur with on the desired angle. In the simulation we got  $\beta l = 35.83$  which is very close to the desired result.  $\beta l$  results are shown positive in the plot, while the actual values are negative since it is an LH band. This is due to software error when choosing the sign of the arccosine function. The Bloch impedance at the desired frequency is also



around the  $Z_B = 50 \Omega$ , this is also what we expected since we aimed to design the unit cell Bloch impedance equal to  $50 \Omega$ .

After when we achieved the unit cell with desired parameters, to obtain the radiation pattern, we should create a periodic structure composed with multiple unit cells. In this way we can achieve higher directivity and gain. To do so, we decided to design three antenna model with different number of unit cells (25, 40 and 50 cells), in this way we can compare the results between three design in terms of efficiency and directivity. While we are analysing the periodic structured antennas models, we should also analyse the dissipated power of each antenna models. The total power dissipated in the LWA, includes the radiated power also the losses due to the conductor and the dielectric. While calculating the dissipated power of each LWA models, we can also compare the percentage of the power dissipated so we can have an idea of how effective our design. The dissipated power can be calculated from the following formula and to see in the graph as a function of frequency, and we can add the following equation in Figure 44 to plot the graph of dissipated power.

$$P_d = 1 - |S_{11}|^2 - |S_{21}|^2 \quad (5.7)$$

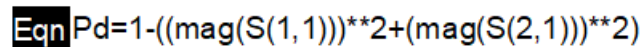


Figure 44 Dissipated Power Equation

It should be noted that the quotient between the radiated power and the total dissipated power is given by the radiation efficiency of the antenna ( $\eta$ ) whose simulated result is shown below. We can start simulating the periodic structured transmission lines, I start with 25-unit cells, in Figure 45 you can see the layout of the 25-unit cell LWA model and in Figure 46 you can observe the results of 25-unit cell LWA transmission line with total length equal to 44,25 cm.

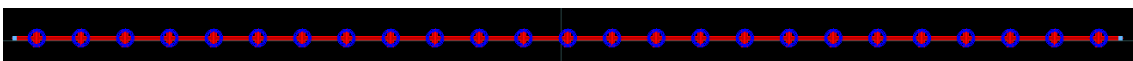


Figure 45 LWA with 25-unit cells layout, with total length 44,25 cm.

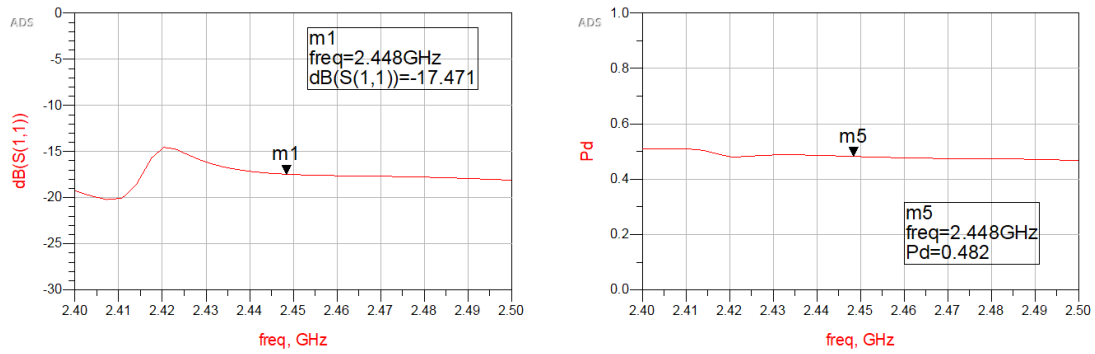


Figure 46 LWA with 25-unit cells characteristics.

As we can see from the Figure 46, our designed LWA has a good matching at the desired frequency (2.44 GHz) reflections lower than -15 dB and the dissipated power is around 48%. In Figure 47, we can also observe the radiation pattern of the antenna at 2.448 GHz.

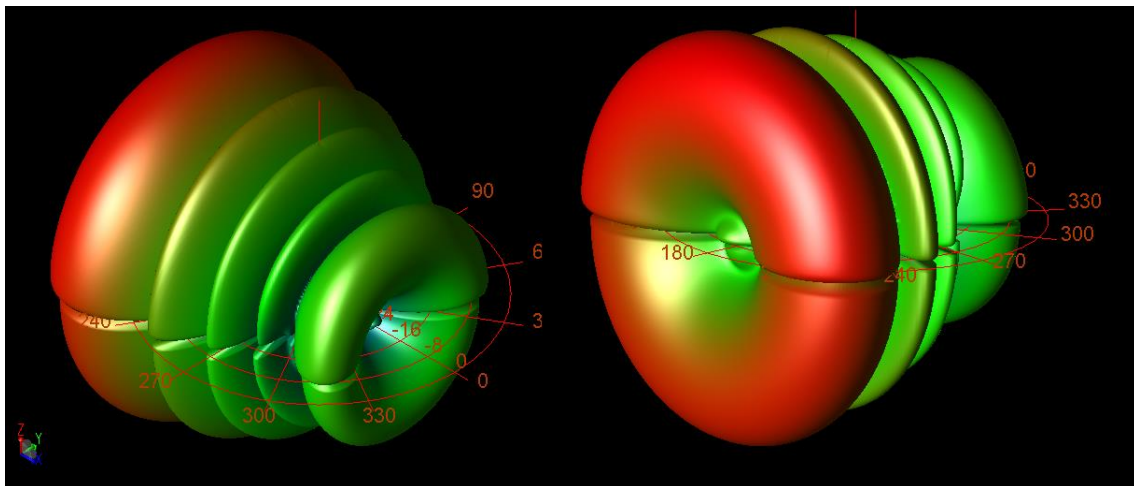


Figure 47 Simulated 3D radiation diagram of the resulting 25 cells LWA, calculated at 2.448 GHz.

In Figure 48, we can observe the directivity and gain values also at the radiation angle of the 25-unit cells LWA model. As we know that, one of the main purposes of this study is to achieve a high directive antenna, so some values of the antenna like directivity, gain and radiation efficiency are important parameters for us.

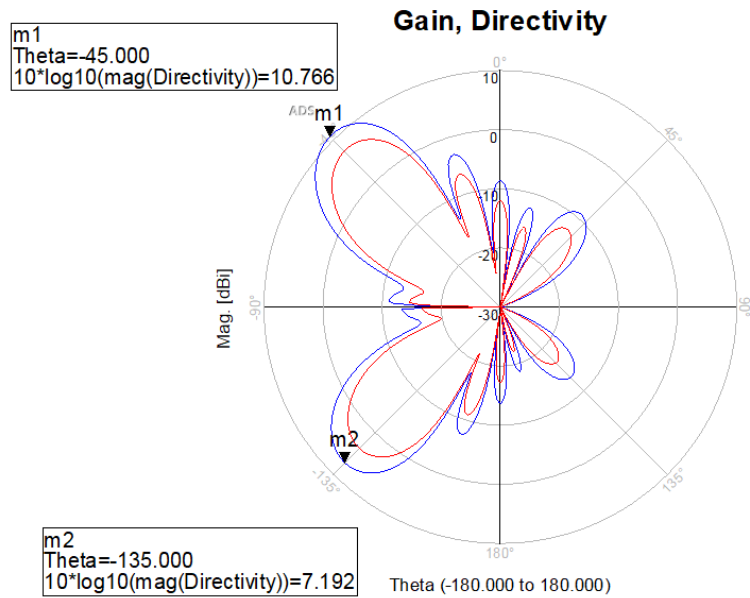


Figure 48 Normalized representation of the gain, directivity and radiation angle of the 25 Unit Cells LWA.

When we examine Figure 48, we can observe that our designed 25-unit cells LWA model has maximum directivity and maximum gain for both angles, at  $\theta = -45^\circ$  as a main lobe and at  $\theta = -135^\circ$  as a secondary lobe, which are exactly radiation angles that we want to achieve. Also, the directivity, gain and radiation efficiency values show that our design has high directivity. However, 25-unit cells LWA model has 48% of dissipated power, this means that our design can just use the 48% of the total power that delivered to antenna. To increase this value and use our design more efficient, basically we can increase the numbers of the unit cells and help to antenna to radiate more power.

When we increase the numbers of unit cells to achieve higher percentage of dissipated power, we design a new LWA model with 40-unit cells. When we simulated the new designed 40-unit cells LWA results can be seen in Figure 49.

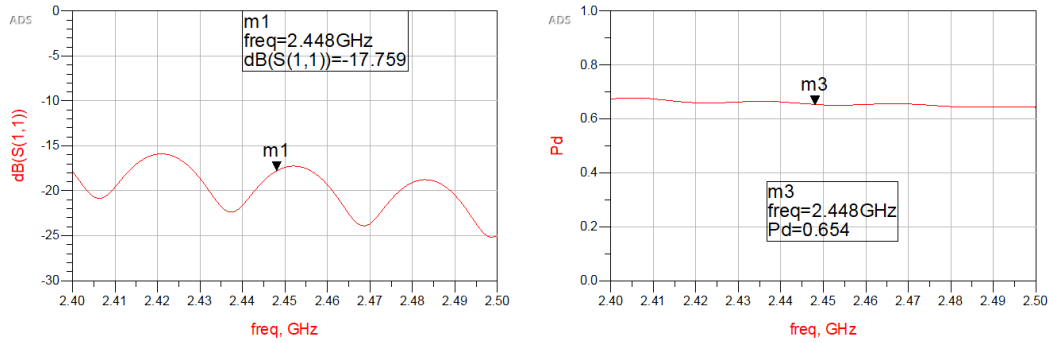


Figure 49 LWA with 40-unit cells characteristics.

From Figure 49, we can observe that our radiations, reflections and the matching at the desired frequency are also good as in 25 cells LWA model. Different than the 25 cells LWA model here in 40 cells LWA, the dissipated power level increased to 65%. In Figure 50, we can observe the radiation pattern of 40-unit cells LWA.

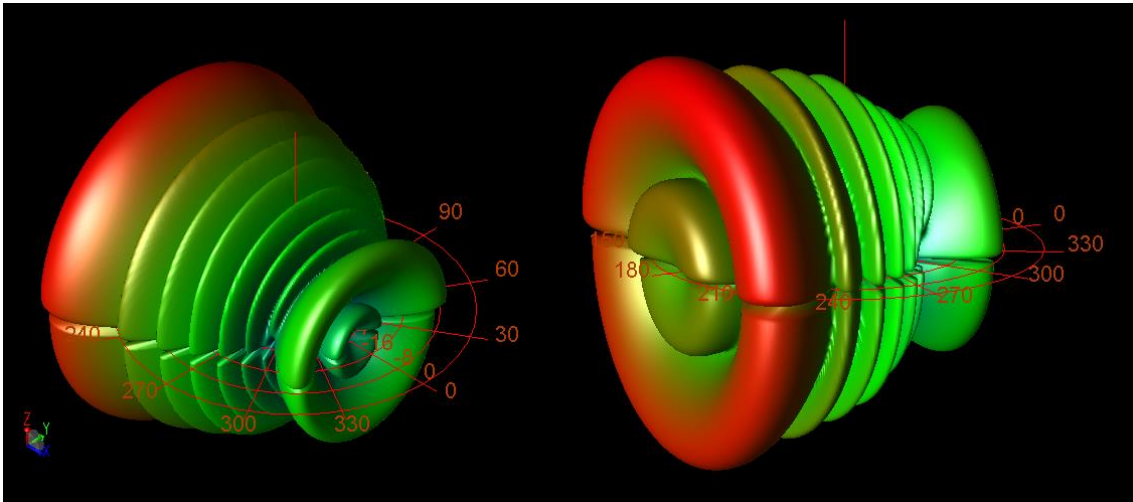


Figure 50 Simulated 3D radiation diagram of the resulting 40 cells LWA, calculated at 2.448 GHz.

In Figure 51, we can observe the 40-unit cells LWA model as improved version of 25-unit cells LWA model in terms of directivity and power dissipated. The radiation angles are the same compare to 25-unit cells LWA, which is normal since we are operating at the same frequency. We can see that the maximum directivity and maximum gain are increased for both angles. However, 40-unit cells LWA model has 65% power dissipated, which is still can be improving to achieve higher level of dissipated power.

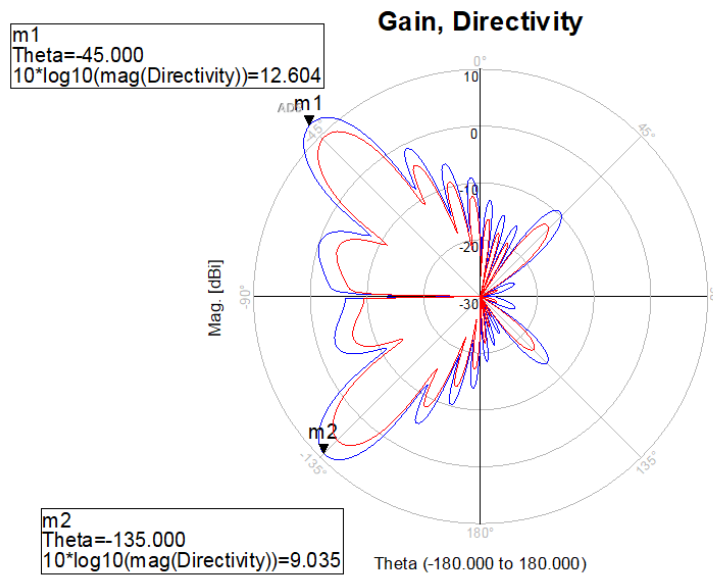


Figure 51 Normalized representation of the gain, directivity and radiation angle of the 40 Unit Cells LWA.

We decided to increase the numbers of unit cells to 50-unit cells. When we simulated the new designed 50-unit cells LWA results can be seen in Figure 52.

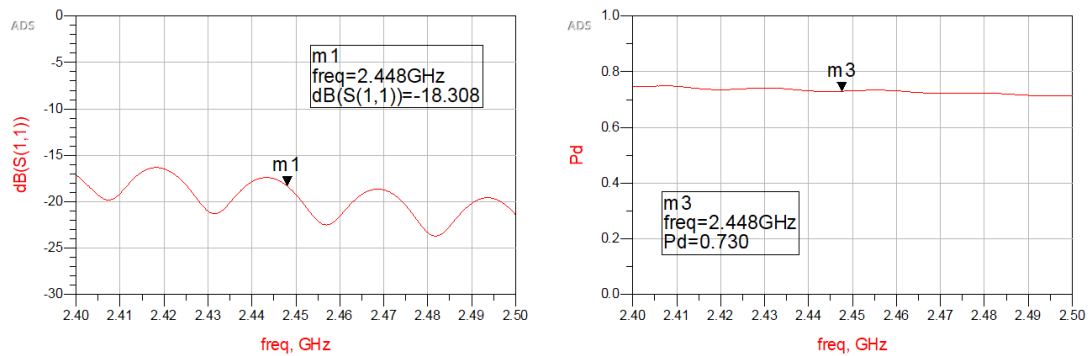


Figure 52 LWA with 50-unit cells characteristics.

From Figure 52, we can observe that our radiations, reflections and the matching are also good at the desired frequency, which are also similar with previous models. In 50 cells LWA model the dissipated power level increased to 74%. In Figure 53, we can observe the radiation pattern of 50-unit cells LWA.

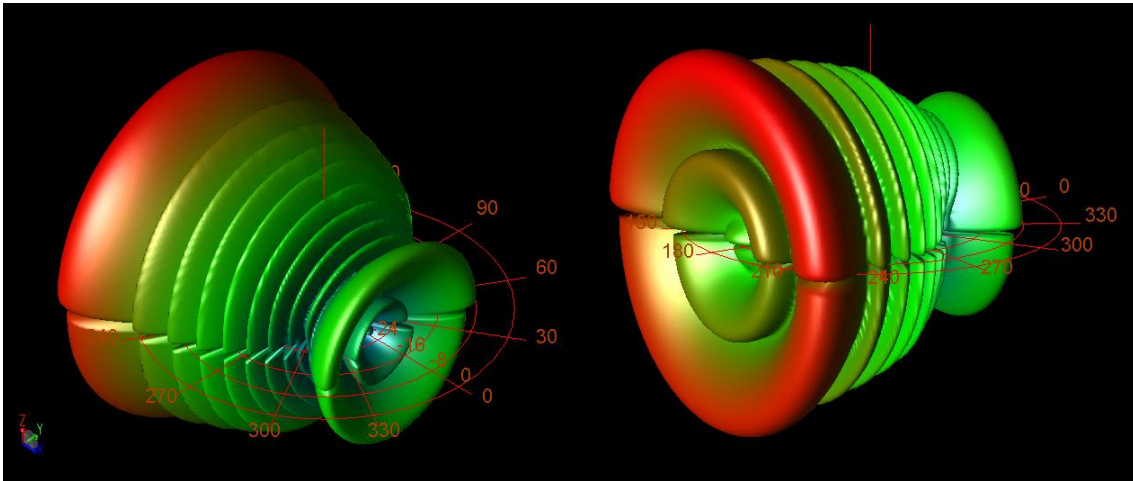


Figure 53 Simulated 3D radiation diagram of the resulting 50 cells LWA, calculated at 2.448 GHz.

In Figure 54, like previous models, 50-unit cell LWA model has the same radiation angles. The maximum directivity and maximum gain are also increased compared to previous models on the both radiation angles. Compare to the previous models 50-unit cells LWA model has 74% of dissipated power, which is much higher value.

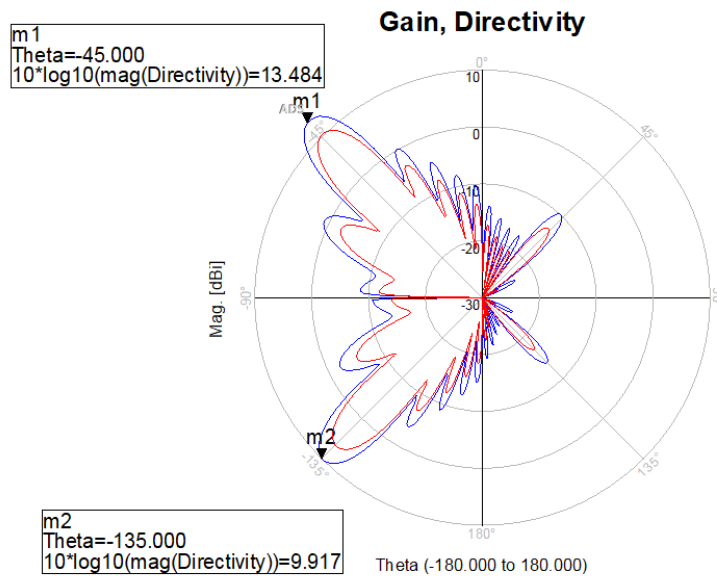


Figure 54 Normalized representation of the gain, directivity and radiation angle of the 50 Unit Cells LWA.

Table 1 shows important parameters of the each LWA model that we designed, while increasing the numbers of the unit cells. We achieved a higher directivity, gain and radiation efficiency values while we are increasing the number of unit cells. Also, increasing the number of unit cells provided us higher level of dissipated power values. From the axial ratio values, we can see that all our LWA designs are linearly polarized.

*Table 1 Comparison Table*

<b>LWA Models</b>	<b>Max Directivity (dB)</b>	<b>Max Gain (dB)</b>	<b>Radiation Efficiency (%)</b>	<b>Dissipated Power (%)</b>	<b>Far Field Border (m)</b>	<b>Axial Ratio (dB)</b>
<b>10 Unit Cells</b>	7.5	3.5	41	24	0.5	14.4
<b>15 Unit Cells</b>	8.7	5.2	44	34	1.2	14.4
<b>25 Unit Cells</b>	10.8	7.3	45	48	3,1	14.4
<b>40 Unit Cells</b>	12.6	9.3	46	65	8,0	14.4
<b>50 Unit Cells</b>	13.5	10.2	46	74	12,5	14.4

As a result, we designed several different lengths of LWA models to achieve high directivity. While we are designing the LWA models we also calculated the far field borders of each antenna model that we simulated. LWA designs can be implemented in several different applications as a very effective solution. For example, to detect certain area with a specific angle like entrance of some factories or any places that requires a detection mechanism for each entry, our designed LWA could be perfect solution. High directivity that LWA can provide with the adjustable radiation angle and wide radiation pattern not only focused to a single point is very special benefits that you can only obtain with LWAs. And while the changing the number of the unit cells we can have LWA with different range of far fields, so it could be easily adaptable to different places, locations or applications.

## 6. Conclusions

In this study, we focused on designing a High directive antenna based on metamaterial technology. To do that, we decided to take advantage of exotic properties of metamaterials to achieve effective media which can behave as a homogeneous media. While using this media we designed periodic structures which can be modified to achieve an antenna that provides high directivity. We decided to use Leaky-Wave Antenna (LWA) in terms of achieving high directivity. Designed LWA works in the LH regime and aimed for the applications can work in short range and low frequencies, like for Bluetooth applications that commonly used in urban environments. Our designed LWA based on microstrip technology composed with CSRRs.

The content of the project has been divided into 4 main chapters. First three chapters are introducing the concepts of metamaterials, effective three-dimensional media and metamaterial transmission lines. The last chapter only focused on LWA and our proposed structure. Regarding the most relevant aspects of each chapter that has a crucial point in this project, to mention briefly that, in chapter two, a brief introduction to the metamaterials has been made, discussing its possible definition and classifying them in electromagnetic crystals or effective media, according to the periodicity of its elementary cells, in terms of wavelength. Special emphasis has been placed on effective media.

In chapter 3, effective three-dimensional media have been explained, beginning with the introduction of resonant particles (SRRs) and their complementary particles (CSRRs). Continuing with the application of SRR and CSRR particles to achieve effective negative permeability (MNG) media ( $\mu_{eff} < 0$ ), effective negative permittivity (ENG) media ( $\epsilon_{eff} < 0$ ) and closing the chapter with the implementation of the LH media by compositing both medias ( $\mu_{eff} < 0$  and  $\epsilon_{eff} < 0$ , simultaneously) and explaining the propagation inside left-handed media, and some of the phenomena that take place in left-handed media.

In Chapter 4, effective planar medias have been studied since easy integration, to planar technologies, wide range of applications where such media can be integrated. The behaviour has been analysed as effective LH media of different transmission lines loaded with split ring resonators (SRR) and complementary split ring resonators (CSRR).



Chapter has been closed analysing the operation of a CRLH transmission lines, whose behave as an effective media varies according to the frequency.

In the last chapter, a Leaky-Wave antenna was introduced, a unit cell and the whole periodic structure designed, simulated and the simulation results analysed. This led us to discussions about the variation of the results obtained during the different numbers of unit cell simulations. While the simulation experiments, we designed some different periodic structures based on different numbers of unit cell LWA models and compared the results between each other. While the comparison of the results, we saw that between all the designs that we simulated had a good matching at desired Bluetooth frequency (2.44 GHz) and radiation angle at desired value ( $-45^\circ$ ) and ( $-135^\circ$ ). Also, directivity that achieved was quite high. Thanks to symmetricity of the radiation pattern of the Leaky-Wave antenna, the design become very useful for many Bluetooth application.

## References

- [1] Shridhar E. Mendhe1, Yogeshwar Prasad Kostas “Metamaterial Properties and Applications”, International Journal of Information Technology and Knowledge Management January-June 2011, Volume 4, No. 1, pp. 85-89.
- [2] I.A. Buriak, V.O. Zhurba, G.S. Vorobjov, V.R. Kulizhko, O.K. Kononov, Oleksandr Rybalko “Metamaterials: Theory, Classification and Application Strategies (Review)”, Journal of Nano and Electronic Physics Vol. 8 No 4(2), 04088(11pp) (2016).
- [3] Kaushal Gangwar, Dr. Paras and Dr. R.P.S. Gangwar "Metamaterials: Characteristics, Process, and Applications", Advance in Electronic and Electric Engineering. ISSN 2231-1297, Volume 4, Number 1 (2014), pp. 97-106.
- [4] N. Katsarakis, T. Koschny, M. Kafesaki, E. N. Economou, and C. M. Soukoulis "Electric coupling to the magnetic resonance of split ring resonators", Appl. Phys. Lett. 84, 2943 (2004).
- [5] F. Martín “Artificial Transmission Lines for RF And Microwave Applications”, pp. 119-148, John Wiley & Sons, Inc., Hoboken, New Jersey, 2015.
- [6] Ricardo MARQUES, Ferran MARTIN, Mario SOROLLA "Metamaterials with Negative Parameters Theory, Design, and Microwave Applications" Published by John Wiley & Sons, Inc., Hoboken, New Jersey.
- [7] Francisco Falcone, Txema Lopetegui, Member, IEEE, Juan D. Baena, Ricardo Marqués, Member, IEEE, Ferran Martín, and Mario Sorolla, Senior Member, IEEE "Effective Negative- $\epsilon$  Stopband Microstrip Lines Based on Complementary Split Ring Resonators" IEEE Microwave and wireless components letters, vol. 14, No. 6 June 2004.
- [8] J. B. Pendry, A. J. Holden, D. J. Robbins, W. J. Stewart, "Magnetism from conductors and enhanced nonlinear phenomena," IEEE Trans. Microwave Theory Tech., vol. 47, no. 11, Nov. 1999.
- [9] Fabrizio Frezza "Introduction to Traveling-Wave antennas", April 18, 2008.
- [10] I. Bahl, P. Bhartia, Microwave solid state circuit design. Wiley, 2nd ed., 2003.

- [11] Cumali Sabah, Fabio Urbani, Savas Uckun "Bloch Impedance Analysis for A Left-Handed Transmission Line", *Journal of Electrical engineering*, VOL. 63, NO. 5, 2012, 310–315.
- [12] "A composite medium with simultaneously negative permeability and permittivity" D. R. Smith, W. J. Padilla, D. C. Vier, S. C. Nemat-Nasser, S. Schultz *Phys. Rev. Lett.* 84, 4184 (2000).
- [13] J. Domingo Baena, J. Bonache, F. Martín, R. Marqués Sillero, F. Falcone, T. Lopetegui, Miguel A. G. Laso, J. García-García, I. Gil, M. Flores Portillo and M. Sorolla "Equivalent-Circuit Models for Split-Ring Resonators and Complementary Split-Ring Resonators Coupled to Planar Transmission Lines", *IEEE transactions on microwave theory and techniques*, vol. 53, no. 4, April 2005.
- [14] Ferran Martín, "Advanced Communications Circuit Design" Course Materials, in *Telecommunications Engineering Master*, Autonomous University of Barcelona.
- [15] Changjun Liu and Kama Huang "Metamaterial Transmission Line and its Applications", *School of Electronics and Information Engineering*, Sichuan University, China.
- [16] Choi J.H., Itoh T. (2016) Beam-Scanning Leaky-Wave Antennas. In: Chen Z., Liu D., Nakano H., Qing X., Zwick T. (eds) *Handbook of Antenna Technologies*. Springer, Singapore
- [17] Keyhan Hosseini and Zahra Atlasbaf "Application of Composite Right/Left-Handed Metamaterials in Leaky-Wave Antennas" February 22nd, 2017
- [18] Muhammad Humza, "ANTENNA LEAKY-WAVE FOR WiMAX APPLICATIONS", Final Work Report of Telecommunications Electronic Engineering Degree, dep. Electronic engineering, Autonomous University of Barcelona, Bellaterra, 2018.
- [19] G.Zamora, S.Zuffanelli, F.Paredes, F. J. Herraiz-Martínez, F. Martín, and J. Bonache: "Fundamental-Mode Leaky-Wave Antenna (LWA) Using Slotline and Split-Ring-Resonator (SRR)-Based Metamaterials"; *IEEE Antennas And Wireless Propagation Letters*, vol. 12, pp.1424-1428, Bellaterra, Spain 2013.